This article has been accepted for publication in a future issue of this journal, but has not been fully edited. Content may change prior to final publication. Citation information: DOI10.1109/JSAC.2022.3196111 IEEE Journal on Selected Areas in Communications

Joint Design of Power Allocation, Beamforming and Positioning for Energy-Efficient UAV-Aided Multiuser Millimeter-Wave Systems

Xiangbin Yu, *Senior Member, IEEE*, Xu Huang, Kezhi Wang, *Senior Member, IEEE*, Feng Shu, and Xiaoyu Dang

***Abstract*—In this paper, the joint design of power allocation (PA), beamforming (BF) and positioning is studied for unmanned-aerial-vehicle (UAV) aided millimeter-Wave (UAV-mmWave) systems, with the objective of maximizing the energy efficiency (EE), under the constraints of maximum transmitting power, minimum data rate from the ground users and positioning range of the UAV. To address the above problem, we first obtain the positioning of the UAV, with the help of approximate beam pattern. Then, near-optimal BF and closed-form PA are derived given the obtained position, with the help of block coordinate descent method. To reduce the complexity, two suboptimal BF schemes with one-loop iteration and closed-form solutions are respectively derived. Furthermore, we propose the simplified algorithms for two special cases, i.e., only line-of-sight (LoS) path and Non-LoS (NLoS) path exist between the users and the UAV. Simulation results verify the effectiveness of the developed joint schemes and show the superior EE performance. Moreover, they can obtain almost the same performance as the existing benchmark schemes but with lower complexity.**

***Index Terms*—Energy efficiency, unmanned aerial vehicle, millimeter-wave communication, power allocation, beamforming design, position optimization.**

I. INTRODUCTION

As the candidate of the next generation spectrum technology, millimeter-wave (mmWave) communication has the advantages of broadband and high speed [1]–[4]. However, the performance of mmWave system is limited by its small wavelength, which suffers from large attenuation in the complex environment [3], [4]. Recently, unmanned Aerial Vehicles (UAVs) have been extensively studied because of its high reliability and flexibility [5], [6]. UAV can not only enhance the transmission performance of cell edge users but also establish temporary communications for specific areas. Moreover, UAV serving as an aerial base station (BS) can increase the coverage and efficiency of the wireless communication when compared to ground BS [7], [8]. Based on this, the mmWave communication and UAV can be effectively combined to improve the overall system performance, and become a promising candidate for future communication because of its high reliability, flexibility and huge bandwidth availability [9].

Up to now, there are several works that have been done to study the performance of mmWave and UAV communications. By means of the proper resources allocation and optimization of UAV deployment, the performance of UAV aided mmWave (UAV-mmWave) communication system can be greatly enhanced. For example, a dynamic resource allocation scheme was proposed for UAV relay assisted mmWave system in [10], where the power allocation (PA) and subcarrier allocation were jointly optimized to maximize the sum rate. In [9], the authors investigated the resource allocation for UAV communications with mmWave massive array antenna, and the scheme of joint PA and user scheduling was designed to maximize the achievable sum rate by using the greedy algorithm. For both works, the deployment of UAV is not optimized. By minimizing the total transmit power under the line-of-sight (LoS) channels, the PA and UAV location were jointly optimized for UAV-assisted multiuser systems with massive MIMO hybrid beamforming in [11], where the optimization problem convexity of UAV position was not proved and mmWave was not considered, and the optimization software tools were used to find the solution, which brings higher complexity. In [12], in order to find the optimal values of the distance and the blocklength, a non-linear optimization problem to minimize the overall decoding error probability was formulated for an ultra-reliable and low-latency (URLLC) aided multi-hop UAV relay links, and a novel, semi-empirical based non-iterative algorithm was proposed to solve the optimization problem. In [13], an UAV and a reconfigurable intelligent surface were applied to deliver short URLLC instruction packets between ground Internet-of-Things (IoT) devices, where UAV position and resource allocation were jointly designed by minimizing the total decoding error rate. Considering the advantage of beamforming (BF) in mmWave system, [14] and [15] studied the BF design. In [14], the multi-UAV enabled mmWave network was investigated to maximize the sum-rate by jointly optimizing the BF and beam-steering, where LoS link was considered. In [15], the coordinated BF design for UAV-aided mmWave systems with

This work was supported in part by the National Natural Science Foundation of China under Grant 62031017, Grant 61971220, and Grant 61971221; in part by the Open Research Fund of State Key Laboratory of Millimeter Waves of Southeast University under Grant K202215.

Xiangbin Yu is with College of Electronic and Information Engineering, Nanjing University of Aeronautics and Astronautics, Nanjing 210016, China, and also with State Key Laboratory of Millimeter Waves of Southeast University, Nanjing 210096, China (e-mail:yxbxwy@gmail.com),

Xu Huang is with College of Electronic and Information Engineering, Nanjing University of Aeronautics and Astronautics, Nanjing 210016, China (e-mail:2958601767@qq.com).

Kezhi Wang is with the Department of Computer and Information Sciences, Northumbria University, Newcastle upon Tyne NE7 7YT, U.K. (e-mail: kezhi.wang@northumbria.ac.uk).

Feng Shu is with the School of Information and Communication Engineering, Hainan University, Hainan 570228, China (e-mail: shufeng0101@163.com).

Xiaoyu Dang is with College of Electronic and Information Engineering, Nanjing University of Aeronautics and Astronautics, Nanjing 210016, China (e-mail:dang@nuaa.edu.cn).

This article has been accepted for publication in a future issue of this journal, but has not been fully edited. Content may change prior to final publication. Citation information: DOI10.1109/JSAC.2022.3196111 IEEE Journal on Selected Areas in Communications

Gaussian process based machine learning was presented, and the compensation beamformer was designed by maximizing the signal-to-interference-plus-noise-ratio. The authors in [16] studied the optimization problem of maximizing the achievable sum rate in multiuser mmWave-UAV system, where the deployment of UAV-BS and BF were jointly optimized to enhance the system performance, but the UAV position was done by two-dimensional (2D) exhaustive search, and BF was attained by the smart algorithm (i.e., artificial bee colony (ABC) algorithm), where the complexity is quite high. In [17], a full-duplex UAV relay system was deployed to improve the mmWave system performance, and positioning, beamforming, and power control were jointly optimized to maximize the achievable rate, where two users were considered, and the standard optimization tools (i.e. CVX) was used to solve the BF design, and 3D search was applied for the position optimization when LoS path is unavailable. The complexity is very high for this solution as well.

Besides, energy efficiency (EE) has become one of the most important performance metrics for wireless communication systems [18], especially for UAV assisted communications whose energy is limited. In [19], the PA and/or subcarrier allocation scheme were presented for UAV-assisted multi-band heterogeneous network to maximize the EE while satisfying the quality of service requirement, and a two-layer optimization framework was proposed to solve the optimization problem. In [20], the quasi-optimization of the sum uplink power of IoT devices communicating to a UAV BS with short data packets was studied, where both UAV position, height, beamwidth, and resource allocation were jointly optimized to enable green URLLC communication. The authors in [21] considered a cellular-enabled UAV network, and proposed two power control schemes based on Q-learning and deep Q-learning to increase the network EE, where a multi-layer deep neural network was used.

Based on the above analysis, the resource allocation schemes for rate maximization in UAV-aided mmWave system were well studied. However, there are few works to address the resource allocation schemes for energy efficient design in UAV-mmWave systems because of the challenging optimization. Specifically, to our best knowledge, an energy-efficient joint design of PA and BF and positioning for multiuser UAV-mmWave systems is not yet available in the literature. Motivated by the reasons above, the EE optimization of multiuser UAV-mmWave for jointly designing the PA and BF as well as positioning over fading channel including LoS and NLoS pathes is studied. Under the constraints of maximum power budget, minimal rate, position range and constant-modulus (CM), the constrained EE optimization problems are formulated. Five suboptimal joint schemes are developed for solving the optimization problem to obtain the corresponding resource allocations. With these schemes, superior EE performance is attained. The main contributions of this paper are summarized as follows:

1) Subject to maximum power, minimum rate, positioning range and CM constraints, a joint PA, BF and positioning optimization problem is firstly formulated for maximizing the EE of a UAV-mmWave system. We propose two-step joint design scheme to tackle this non-convex problem, where we optimize the position, and then optimize BF and PA. Specifically, we firstly transform the original problem into the design of beam gain, position and PA by utilizing the approximate beam pattern. Then, considering the block structure of this transformed problem, we use the block coordinate descent (BCD) method to solve it. Given the position and PA, the optimal beam gain with closed-form is derived, and given the PA and beam gain, suboptimal position of UAV is attained. Also, closed-form approximate position is derived for special path exponent. Based on the obtained beam gain and position, the optimal PA with closed form is derived. With these results, a near-optimal joint beam gain, positioning and PA design is developed with BCD method, and corresponding position optimization is attained.

2) With the obtained UAV position above, the original problem is reduced to a joint BF and PA problem. An effective iterative algorithm is proposed to tackle this problem by using the penalty function and the BCD method, where near-optimal BF is derived, which has closed-form solution for each iteration. However, this algorithm needs three-loop iteration. To lower the complexity, two suboptimal BF schemes are derived. The first one is based on the obtained beam gain at the first step, which only needs a single-loop iteration. The second one is based on the obtained PA at the first step, and it has closed-form solution. Hence, they have lower complexity than the near-optimal BF, where only small performance gap is found. Thus, the corresponding joint schemes can realize the effective tradeoff between the performance and complexity.

3) Considering that the joint schemes above need two-step optimization, the complexity is relatively higher. For this reason, we present one-step joint optimization of BF, PA and position under two special cases, i.e., only LoS path or NLoS path exists. Under these two cases, the joint optimization of the BF, PA and position can be optimized directly, and do not need two-step optimization. Based on this, using the analytical method of above joint schemes and the BCD method, the joint schemes for two special cases are developed, and corresponding algorithm is presented, which will lower the complexity. Simulation results show the effectiveness of the proposed joint schemes.

Notations: In this paper, $(\cdot)^*$, $(\cdot)^T$ and $(\cdot)^H$ stand for the complex conjugate, the transpose and conjugate transpose, respectively. Vectors and matrices are represented by boldface lower-case and upper-case symbols, respectively. $|\cdot|$ represents the absolute value. $\mathrm{Re}\{\cdot\}$ means taking the real part. $\mathcal{O}(\cdot)$ stands for the big-O notation. $\vec{\lambda}_{\max}(\cdot)$ gives the eigenvector of the maximum eigenvalue of a Hermitian matrix. Besides, $\mathrm{U}[a,b]$ represents the uniform distribution in the interval $[a,b]$, $\mathcal{CN}(0,\sigma^2)$ denotes the complex Gaussian distribution with zero mean and variance σ^2.

II. SYSTEM MODEL

In this paper, we consider a downlink UAV-mmWave communication system with multiple ground users, as shown in Fig.1, where one UAV is deployed as a flying BS and serves K users with single antenna. The UAV-BS is equipped with

This article has been accepted for publication in a future issue of this journal, but has not been fully edited. Content may change prior to final publication. Citation information: DOI10.1109/JSAC.2022.3196111 IEEE Journal on Selected Areas in Communications

an M-element uniform linear array (ULA) and located at (x_0, y_0, H_u), where $x \in [x_{min}, x_{max}]$ and $y \in [y_{min}, y_{max}]$, H_u is the flying altitude and is set as a constant for safety consideration. The users are distributed on the horizontal plane with 2-D rectangular area, i.e., user k is located at $(x_k, y_k, 0)$ with $x_{min} \le x_k \le x_{max}$ and $y_{min} \le y_k \le y_{max}$ for $k = 1, ..., K$. The UAV employs the phased antenna array with analog BF structure, where all the M antennas are connected to a radio frequency (RF) chain, and each antenna branch has a phase shifter with a power amplifier to drive the antenna [22], [23]. These antennas have the same power amplification factor in general. Thus, the BF vector $\mathbf{w}$ has CM elements i.e., $|[\mathbf{w}]_m| = 1/\sqrt{M}$, where $m = 1, ..., M$. The channels assigned to different users are orthogonal or non-overlapped [24], [25], [16], and thus there is no interference between the users. Then, the received signal of the k-th ground user can be written as

$$y_k = \sqrt{p_k}\mathbf{h}_k^H \mathbf{w} s_k + n_k, \tag{1}$$

where $p_k \ge 0$ is the transmit power from the UAV to user k, s_k is the transmission signal to user k with unit energy, n_k is the complex Gaussian noise with zero mean and variance σ^2. $\mathbf{h}_k$ is the mmWave channel vector between the UAV-BS and user k, which can be modeled as [22], [23], [16], [26]–[28],

$$\mathbf{h}_k = \sum\nolimits_{l=0}^{L_k} \beta_{k,l}\mathbf{a}(M, \theta_{k,l}), \tag{2}$$

where L_k+1 is the number of the channel paths between the UAV and user k, $\beta_{k,l}$ and $\theta_{k,l}$ are the channel gain and the angle of departure (AoD) of the l-th path, respectively, $\mathbf{a}(\cdot)$ denotes the steering vector function given as

$$\mathbf{a}(M, \theta) = [e^{j\pi 0 \cos\theta}, e^{j\pi 1 \cos\theta}, \cdots, e^{j\pi(M-1)\cos\theta}], \tag{3}$$

where $\theta \sim \mathrm{U}[0, 2\pi]$. According to [28]–[30], [16], equation (3) can be further written as

$$\mathbf{h}_k = \mathbf{h}_k^{Los} + \mathbf{h}_k^{Nlos} = \beta_{k,0}\mathbf{a}(M, \theta_{k,0}) + \sum\nolimits_{l=1}^{L_k} \beta_{k,l}\mathbf{a}(M, \theta_{k,l}), \tag{4}$$

where $\mathbf{h}_k^{Los}$ and $\mathbf{h}_k^{Nlos}$ are LoS and non-line-of-sight (NLoS) components of channels, respectively. For the LoS component, the channel gain $\beta_{k,0}$ can be expressed as $\beta_{k,0} = \lambda_0 d_k^{-\alpha_{Los}/2}/(4\pi)$ [31] [16], where $\lambda_0 = c/f_c$ is the wavelength and f_c is the carrier frequency, α_{Los} is the LoS path loss exponent, $d_k = \sqrt{(x_0 - x_k)^2 + (y_0 - y_k)^2 + H_u^2}$ is the propagation distance between the UAV and user k, which includes the effect of the UAV's position. For the NLoS component, the channel gain $\beta_{k,l}$ can be written as $\beta_{k,l} = \xi_{k,l}\lambda_0(4\pi)^{-1}d_k^{-\alpha_{Nlos}/2}/\sqrt{L_k}$ according to [28] and [29], where $\xi_{k,l} \sim \mathcal{CN}(0,1)$, α_{Nlos} is the NLoS path loss exponent.

With (1), the achievable transmission rate of ground user k can be given by

$$R_k = \log_2(1 + p_k|\mathbf{w}^H\mathbf{h}_k|^2/\sigma^2). \tag{5}$$

Thus, the sum rate of the system is obtained as

$$R = \sum\nolimits_{k=1}^{K} R_k = \sum\nolimits_{k=1}^{K} \log_2(1 + p_k|\mathbf{w}^H\mathbf{h}_k|^2/\sigma^2). \tag{6}$$

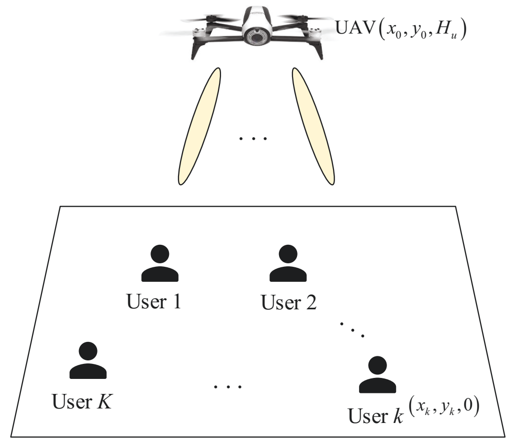

Fig. 1. Structure of multiuser UAV-mmWave system

According to the definition of energy efficiency, using (6), the EE of the multiuser UAV-mmWave system can be expressed as

$$\eta_{EE} = \frac{\sum_{k=1}^{K} \log_2(1 + p_k|\mathbf{w}^H\mathbf{h}_k|^2/\sigma^2)}{\varrho\sum_{k=1}^{K} p_k + P_c}, \tag{7}$$

where $\varrho = 1/\kappa$, $\kappa \in (0, 1]$ is the drain efficiency of power amplifiers. P_c is a fixed circuit power consumption, which is given by $P_{BB} + P_{RF} + MP_{PS}$, where P_{BB}, P_{RF} and P_{PS} are the power consumptions of the baseband, the RF chain and the phase shifter, respectively [16], [32]. The transmit powers $\{p_k\}$ are constrained by $\sum_{k=1}^{K} p_k \le P_{max}$, where P_{max} is the maximum transmit power available at the UAV-BS.

With (7), under the constraints of maximum power, each user's minimum rate and positioning range, the optimization problem on maximizing EE can be formulated as:

$$\begin{aligned} \max_{\mathbf{p},\mathbf{w},x_0,y_0} \ & J_1 = \frac{\sum_{k=1}^{K} \log_2(1 + p_k|\mathbf{w}^H\mathbf{h}_k|^2/\sigma^2)}{\varrho\sum_{k=1}^{K} p_k + P_c} \\ \text{s.t.} \ & C_1 : \sum\nolimits_{k=1}^{K} p_k \le P_{max}, \\ & C_2 : R_k \ge r_0 \\ & C_3 : |[\mathbf{w}]_m| = 1/\sqrt{M}, \ m = 1, \ldots, M, \\ & C_4 : x_{min} \le x_0 \le x_{max}, \ y_{min} \le y_0 \le y_{max}, \end{aligned} \tag{8}$$

where $\mathbf{p} = [p_1, p_2, \ldots, p_K]^T$, r_0 is the minimum rate constraint of users. From (8), it can be easily known that the constraints C_2 and C_3 are non-convex according to the definition of the convex set. Thus, the above joint optimization problem is a non-convex fractional one, and can be solved by means of multi-dimensional exhaustive search methods, but the computational complexity is extremely high. This is because the real optimization variables that needs to be jointly searched are $2M + K + 2$, and the number is very large in general. Beside, these optimization variables are coupled with each other, which will result in the huge difficulty of solving optimization problem. For these reason, we will use two-step optimization method to tackle the above problem. Firstly, we use the approximate beam pattern method [22] [16] to simply the optimization design of position. Namely, by optimizing

This article has been accepted for publication in a future issue of this journal, but has not been fully edited. Content may change prior to final publication. Citation information: DOI10.1109/JSAC.2022.3196111 IEEE Journal on Selected Areas in Communications

the EE, the position of UAV, PA of users and beam gain are jointly designed to obtain the suboptimal position, which will be introduced in Section III. Secondly, based on the obtained UAV position, we jointly design the BF and PA to obtain the suboptimal solution, which will be shown in Section IV.

III. Position optimization for UAV-mmWave system

In this section, to solve the problem (8), we firstly give the position optimization of UAV, which will facilitate the development for the subsequent joint design of the beamforming and power allocation.

According to the analysis in [22] and [16], for each user, the UAV-BS performs BF toward the angle direction along the strongest multipath component (MPC) to achieve high array gain. This is based on the fact that the number of the MPC in mmWave channel is small in general, and the mmWave channel has directionality and spatial sparsity in the angle domain. Let $|\beta_k| = \max_l |\beta_{k,l}|$, then the effective channel gain is approximated as [22] [16]

$$|\mathbf{w}^H \mathbf{h}_k|^2 \approx |\beta_k|^2 b_k = |\beta_k|^2 |\mathbf{w}^H \mathbf{a}_k|^2, \tag{9}$$

where $b_k = |\mathbf{w}^H \mathbf{a}_k|^2$ is the beam gain of user k. According to the Lemma 1 in [16] and [22], the beam gains $\{b_k\}$ satisfy that the summation is M, i.e., $\sum_{k=1}^K b_k = M$.

Based on the analysis above, the optimization problem (8) can be transformed into

$$\begin{aligned} \max_{\mathbf{p},\mathbf{b},x_0,y_0} \ & J_2 = \frac{\sum_{k=1}^K \log_2(1 + p_k |\beta_k|^2 b_k / \sigma^2)}{\varrho \sum_{k=1}^K p_k + P_c} \\ \text{s.t.} \ \ & C_1, C_4, \\ & \tilde{C}_2 : p_k |\beta_k|^2 b_k / \sigma^2 \geq \rho_0, \\ & C_5 : \sum_{k=1}^K b_k = M, \end{aligned} \tag{10}$$

where $\mathbf{b} = [b_1, \ldots, b_K]^T$, $\rho_0 = 2^{r_0} - 1$ is from the constraint C_2. Taking both the maximum power and the minimum rate constraints into account, i.e., C_1 and C_2, the above optimization problem may have no feasible solution when the maximum power limitation is small and/or channel conditions are poor. In case of no feasible solution, the communication will be suspended. Hence, we need to determine whether problem (10) has feasible solution. For this reason, we give the feasibility analysis of (10) in Appendix A.

After further observation, it is found from (10) that three optimization variables **p**, **b** and (x_o, y_o) can be respectively optimized. In other words, given two variables, another variable can be determined. Moreover, these variables have block structure. Based on this, we can exploit the BCD method [33]-[34] to tackle the problem (10) considering the effectiveness of this method.

A. Solve the subproblem with respect to b for fixed p and position

Given the PA **p** and location (x_0, y_0) (corresponding $|\beta_k|^2$ is given), beam gain **b** is related to the numerator of objective function in (10) and constraints $\tilde{C}_2, C_5$. Based on this, the subproblem with respect to (w.r.t) **b** is formulated as

$$\begin{aligned} \max_{\mathbf{b}} \ & J_3 = \sum_{k=1}^K \log_2(1 + p_k |\beta_k|^2 b_k / \sigma^2) \\ \text{s.t.} \ & \tilde{C}_2, C_5, \end{aligned} \tag{11}$$

For problem (11), the objective function is concave, and the constrains are linear, therefore it is convex. Thus, (11) has global solution. Hence, it can be tackled by the standard optimization tools, like CVX software. However, these optimization tools have high computational complexity and low efficiency in general. For this reason, we use the Lagrange multiplier method to solve the problem (11). Besides, taking minimum rate constraint into account, the above optimization problem may have no feasible solution when the channel conditions are worse and maximum power P_{max} is smaller. Considering the constrains $\tilde{C}_2$ and C_5, the antenna number needs to satisfy that $M \geq \sum_{k=1}^K \frac{\sigma^2 \rho_0}{p_k |\beta_k|^2}$. Otherwise, the feasible region is null.

According to the analysis above, under the constraint C_5, the Lagrange function is given by

$$\mathcal{L}_1 = \sum_{k=1}^K \log_2(1 + p_k |\beta_k|^2 b_k / \sigma^2) + \mu(M - \sum_{k=1}^K b_k) \tag{12}$$

where μ is the Lagrange multiplier. By setting $\partial \mathcal{L}_1 / \partial b_k = 0$, we can obtain:

$$b_k = \frac{1}{\mu \log 2} - \frac{\sigma^2}{p_k |\beta_k|^2}. \tag{13}$$

Substituting (13) into the constraint condition $\sum_{k=1}^K b_k = M$ yields the closed-form solution of b_k as

$$b_k = \frac{M}{K} + \frac{1}{K} \sum_{i=1}^K \frac{1}{g_i} - \frac{1}{g_k}, \tag{14}$$

where $g_k = p_k |\beta_k|^2 / \sigma^2$. Hence, when g_k is small, b_k is also small. Based on this, for the users with small g_k, their rate may not meet the requirement of r_0. For this reason, we need to set these users' rate equals to r_0 to obtain the corresponding beam gains. Hence, by sorting g_k in descending order (i.e., $g_1 > ... > g_K$), the $\{b_k\}$ can be rewritten as

$$\begin{aligned} b_k = \ & \frac{M - \sum_{i=K_0+1}^K \rho_0 g_i^{-1}}{K_0} + \frac{1}{K_0} \sum_{i=1}^{K_0} \frac{1}{g_i} - \frac{1}{g_k}, k = 1, ..., K_0, \\ \text{and} \ \ & b_k = \rho_0 / g_k, \qquad\qquad k = K_0 + 1, ..., K, \end{aligned} \tag{15}$$

where K_0 can be determined by the following procedure.

Let $U_n = \sum_{i=1}^n g_i^{-1}$ and $V_n = \sum_{i=n+1}^K \rho_0 g_i^{-1}$. Starting from $n = K$, compute $b_n(g_n) = \frac{M - V_n}{n} + \frac{U_n}{n} - \frac{1}{g_n}$. If $r_n = \log_2(1 + g_n b_n(g_n)) \geq r_0$, then $K_0 = n$. Otherwise, compute $U_{n-1} = U_n - g_n^{-1}$, $V_{n-1} = V_n + \rho_0 g_n^{-1}$, and set $n = n - 1$, and then repeat the calculation of r_n until it is not less than r_0.

B. Solve the subproblem w.r.t (x_0, y_0) for fixed b and p

Given the beam gain **b** and PA **p**, the location (x_0, y_0) is related to the numerator of objective function in (10) and constraints C_4 and C_2. Therefore, the subproblem w.r.t (x_0, y_0) is formulated as

$$\begin{aligned} \max_{x_o,y_o} J_4 &= \sum\nolimits_{k=1}^{K} \log_2(1+p_k\phi_k d_k^{-\alpha} b_k/\sigma^2) \\ \text{s.t. } & C_6 : \phi_k d_k^{-\alpha} p_k b_k \geq \sigma^2 \rho_0, \\ & C_4, \end{aligned} \tag{16}$$

where $|\beta_k|^2 = \phi_k d_k^{-\alpha}$, $\alpha = \alpha^{Los}$ and $\phi_k = (\lambda_0/(4\pi))^2$ when LoS is selected, $\alpha = \alpha^{Nlos}$ and $\phi_k = \lambda_0^2 |\xi_{k,l^*}|^2/((4\pi)^2 L_k)$ when NLoS is selected, in which l^* is the index of the strong path. $d_k = [(x_0-x_k)^2+(y_0-y_k)^2+H_u^2]^{1/2}$. For the problem (16), we can use the 2D search to find the optimal solution of UAV position, such as [16], but the complexity is still high. For this reason, we give a simple calculation method to obtain the solution below.

Let $T_k = p_k\phi_k b_k/\sigma^2$, then $J_4 = \sum_{k=1}^{K} \log_2(1+T_k d_k^{-\alpha})$. Hence, we can maximize J_4 to obtain the solution of UAV position, but the solution is not easily obtained due to the non-convexity of problem. Considering that the objective function J_4 is lower bounded by J_4^L=$\log_2(1+\sum_{k=1}^{K} T_k d_k^{-\alpha})$, we can maximize this bound to obtain suboptimal solution. Moreover, maximizing J_4^L is equivalent to

$$\max_{x_o,y_o} J_5 = \sum\nolimits_{k=1}^{K} T_k d_k^{-\alpha}. \tag{17}$$

Furthermore, (17) is equivalent to

$$\min_{x_o,y_o} \tilde{J}_5 = \frac{1}{\sum_{k=1}^{K} T_k d_k^{-\alpha}}. \tag{18}$$

According to the arithmetic-geometric means inequality in [35], we have:

$$\begin{aligned} \frac{1}{\sum_{i=1}^{n} a_i} &\leq \frac{1}{n}\frac{1}{(\prod_{i=1}^{n} a_i)^{1/n}} = \frac{1}{n}(\prod_{i=1}^{n}\frac{1}{a_i})^{\frac{1}{n}} \\ &\leq \frac{1}{n^2}\sum\nolimits_{i=1}^{n}\frac{1}{a_i} \leq \sum\nolimits_{i=1}^{n}\frac{1}{a_i} \end{aligned} \tag{19}$$

With (19), $\frac{1}{\sum_{k=1}^{K} T_k d_k^{-\alpha}}$ in (18) is upper bounded by $\sum_{k=1}^{K}\frac{1}{T_k d_k^{-\alpha}}$, so we can minimize this upper bound to obtain approximate solution, i.e.,

$$\min_{x_0,y_0} \mathcal{F} = \sum\nolimits_{k=1}^{K} d_k^{\alpha}/T_k. \tag{20}$$

For (20), taking the derivative of $\mathcal{F}$ w.r.t x_0 and y_0 respectively yields

$$\begin{aligned} \partial\mathcal{F}/\partial x_0 &= \sum\nolimits_{k=1}^{K} \alpha(x_0-x_k) d_k^{\alpha-2} T_k^{-1} \\ \partial\mathcal{F}/\partial y_0 &= \sum\nolimits_{k=1}^{K} \alpha(y_0-y_k) d_k^{\alpha-2} T_k^{-1}. \end{aligned} \tag{21}$$

With (21), we have:

$$\begin{aligned} \frac{\partial^2\mathcal{F}}{\partial x_0^2} &= \sum_{k=1}^{K}\frac{\alpha d_k^{\alpha-2}}{T_k} + \sum_{k=1}^{K}\frac{\alpha(\alpha-2)(x_0-x_k)^2 d_k^{\alpha-4}}{T_k}, \\ \frac{\partial^2\mathcal{F}}{\partial y_0^2} &= \sum_{k=1}^{K}\frac{\alpha d_k^{\alpha-2}}{T_k} + \sum_{k=1}^{K}\frac{\alpha(\alpha-2)(y_0-y_k)^2 d_k^{\alpha-4}}{T_k}, \\ \frac{\partial^2\mathcal{F}}{\partial x_0 y_0} &= \frac{\partial^2\mathcal{F}}{\partial y_0 x_0} = \sum_{k=1}^{K}\frac{\alpha(\alpha-2)(x0-x_k)(y_0-y_k) d_k^{\alpha-4}}{T_k}, \end{aligned} \tag{22}$$

and correspondingly, the Hessian matrix of $\mathcal{F}$ is expressed as

$$H_{\mathcal{F}} = \begin{bmatrix} \frac{\partial^2\mathcal{F}}{\partial x_0^2} & \frac{\partial^2\mathcal{F}}{\partial x_0 y_0} \\ \frac{\partial^2\mathcal{F}}{\partial y_0 x_0} & \frac{\partial^2\mathcal{F}}{\partial y_0^2} \end{bmatrix}. \tag{23}$$

Utilizing the Cauchy-Schwarz inequality: $(\sum_{k=1}^{K} a_k b_k)^2 \leq \sum_{k=1}^{K} a_k^2 \sum_{k=1}^{K} b_k^2$, we can prove that the determinant of $H_{\mathcal{F}}$, $\det(H_{\mathcal{F}}) > 0$. Moreover, the first element of $H_{\mathcal{F}}$ is $\frac{\partial^2\mathcal{F}}{\partial x_0^2} > 0$. Therefore, the Hessian matrix $H_{\mathcal{F}}$ is positive definite. Thus, the problem (20) is convex, and has the global optimal solution. Based on this, by setting $\partial\mathcal{F}/\partial x_0 = 0$ and $\partial\mathcal{F}/\partial y_0 = 0$, we respectively have:

$$\begin{aligned} x_0 \sum\nolimits_{k=1}^{K} d_k^{\alpha-2} T_k^{-1} &= \sum\nolimits_{k=1}^{K} x_k d_k^{\alpha-2} T_k^{-1}, \\ y_0 \sum\nolimits_{k=1}^{K} d_k^{\alpha-2} T_k^{-1} &= \sum\nolimits_{k=1}^{K} y_k d_k^{\alpha-2} T_k^{-1}. \end{aligned} \tag{24}$$

Hence, we can use the fixed point iteration method to obtain the optimal solution (x_0^*, y_0^*), which is also the suboptimal solution of the original problem (16). Since $x_k \in [x_{min}, x_{max}]$ and $y_k \in [y_{min}, y_{max}]$, according to (24), we can easily obtain that $x_0^* \in [x_{min}, x_{max}]$ and $y_0^* \in [y_{min}, y_{max}]$. Namely, the obtained solution can satisfy the range of position. Considering that the above solution needs iteration, we give a closed-form solution for special path-loss exponent, i.e., α equals 2, which is often used for LoS component in mmWave system [10], [19], [36]. When α=2, the closed-form solution is

$$\begin{aligned} x_0^* &= \sum\nolimits_{k=1}^{K} x_k T_k^{-1} \Big/ \sum\nolimits_{k=1}^{K} T_k^{-1}, \\ y_0^* &= \sum\nolimits_{k=1}^{K} y_k T_k^{-1} \Big/ \sum\nolimits_{k=1}^{K} T_k^{-1}. \end{aligned} \tag{25}$$

Moreover, when K=1, the above solution is also the optimal one for (16) since no approximation of objective function is used. With the obtained solution (x_0^*, y_0^*), the available rate of user may not meet the requirement of minimal rate. Under this case, we can set the user's rate equal to r_0 to obtain the required power. Thus, the maximization of EE becomes the minimization of total power, i.e.,

$$\begin{aligned} \min_{x_0,y_0} J_6 &= P_t = \sum\nolimits_{k=1}^{K} \frac{\sigma^2\rho_0 d_k^{\alpha}}{\phi_k b_k} \\ \text{s.t. } & C_4, \end{aligned} \tag{26}$$

where $P_t = \sum_{k=1}^{K} p_k$ is the power to meet r_0, and $p_k = \sigma^2\rho_0 d_k^{\alpha}/(\phi_k b_k)$ is from the constraint C_6. Using the analytical method in problem (20), we can prove that the problem (26) is also convex, and thus it has the global optimal solution. By setting $\partial J_6/\partial x_0 = 0$ and $\partial J_6/\partial y_0 = 0$, the optimal solution of (x_0, y_0) for problem (26) is attained as

$$\begin{aligned} x_0 \sum\nolimits_{k=1}^{K} \frac{d_k^{\alpha-2}}{(\phi_k b_k)} &= \sum\nolimits_{k=1}^{K} \frac{x_k d_k^{\alpha-2}}{(\phi_k b_k)}, \\ y_0 \sum\nolimits_{k=1}^{K} \frac{d_k^{\alpha-2}}{(\phi_k b_k)} &= \sum\nolimits_{k=1}^{K} \frac{y_k d_k^{\alpha-2}}{(\phi_k b_k)}. \end{aligned} \tag{27}$$

Based on (27), we can employ the fixed point iteration method to obtain the optimal solution (x_0^*, y_0^*) of problem

This article has been accepted for publication in a future issue of this journal, but has not been fully edited. Content may change prior to final publication. Citation information: DOI10.1109/JSAC.2022.3196111 IEEE Journal on Selected Areas in Communications

(26). For (27), when $\alpha = 2$, the closed-form solution can be obtained, i.e.,

$$\begin{aligned} x_0^* &= \sum\nolimits_{k=1}^{K} x_k (\phi_k b_k)^{-1} / \sum\nolimits_{k=1}^{K} (\phi_k b_k)^{-1}, \\ y_0^* &= \sum\nolimits_{k=1}^{K} y_k (\phi_k b_k)^{-1} / \sum\nolimits_{k=1}^{K} (\phi_k b_k)^{-1}. \end{aligned} \tag{28}$$

Under this case, the obtained total power may be beyond the maximum power for bad channel conditions, and the feasible solution may not exist.

Based on the analysis above, we can obtain the suboptimal position of UAV-BS for the original problem (8), and closed-form position is also attained for special path-loss exponent of $\alpha = 2$, which will benefit the deployment of UAV. Thus, the multidimensional search in the existing references is avoided and the complexity is reduced.

C. Solve the subproblem w.r.t $\mathbf{p}$ *for fixed* $\mathbf{b}$ *and position*

Given the beam gain $\mathbf{b}$ and location (x_0, y_0) (corresponding $|\beta_k|^2$ is given), the PA $\mathbf{p}$ is related to the objective function in (10) and constraints C_1 and $\tilde{C}_2$. Based on this, the subproblem w.r.t $\mathbf{p}$ is formulated as

$$\begin{aligned} &\max_{\mathbf{p}} J_7 = \frac{\sum_{k=1}^{K} \log_2(1 + p_k |\beta_k|^2 b_k / \sigma^2)}{\varrho \sum_{k=1}^{K} p_k + P_c} \\ &\text{s.t.} \quad C_1, \quad \tilde{C}_2, \end{aligned} \tag{29}$$

It is observed that the denominator in (29) is an affine function and the numerator is a concave function, while the constraint is linear. Thus, the problem (29) is strictly pseudo-convex, and will have a global solution. Hence, this problem can be well tackled by the CVX software, but the complexity is much higher. Considering the maximum power constraint C_1 and minimal rate constraint C_2, P_{max} needs to satisfy that $P_{max} \geq \sum_{k=1}^{K} \frac{\sigma^2 \rho_0}{b_k |\beta_k|^2}$. Otherwise, the feasible region is empty.

Since (29) is a fractional problem, we can utilize the fractional programming (FP) theory [37] to attain the optimal solution. Correspondingly, (29) is changed to an equivalent subtraction problem, i.e.,

$$\begin{aligned} \max_{\mathbf{p}} J_8 = &\sum\nolimits_{k=1}^{K} \log_2(1 + p_k |\beta_k|^2 b_k / \sigma^2) \\ &- \varpi(\varrho \sum_{k=1}^{K} p_k + P_c) \\ \text{s.t.} \quad &C_1, \quad \tilde{C}_2, \end{aligned} \tag{30}$$

where ϖ is a non-negative parameter. Let $\mathcal{F}(\varpi)$=$\max_{\mathbf{p}} J_8(\mathbf{p}, \varpi)$. It has been proved that the problems (30) and (29) are equivalent if and only if $\mathcal{F}(\varpi^*)$=0 in terms of FP [37]. Thus, the problems (30) and (29) have the same solution. Therefore, we only need to optimize the equivalent problem (30) in order to achieve the solution of (29). Considering the constraint C_1, the Lagrangian of (30) is given by

$$\begin{aligned} &\max_{\mathbf{p}} J_9 = \sum\nolimits_{k=1}^{K} \log_2(1 + p_k |\beta_k|^2 b_k / \sigma^2) \\ &-\varpi(\varrho \sum\nolimits_{k=1}^{K} p_k + P_c) + \nu(P_{max} - \sum\nolimits_{k=1}^{K} p_k), \end{aligned} \tag{31}$$

where ν is the Lagrange multiplier. With (31), the derivative of J_9 w.r.t. p_k can be calculated as

$$\frac{\partial J_9}{\partial p_k} = \frac{b_k |\beta_k|^2}{(\sigma^2 + p_k |\beta_k|^2 b_k) \log 2} - \varpi \varrho - \nu. \tag{32}$$

By setting $\partial J_9 / \partial p_k = 0$, the optimal power can be attained as

$$p_k = \frac{1}{(\varpi \varrho + \nu) \log 2} - \frac{\sigma^2}{|\beta_k|^2 b_k}. \tag{33}$$

With (33), we have:

$$p_1 + \frac{\sigma^2}{|\beta_1|^2 b_1} = p_2 + \frac{\sigma^2}{|\beta_3|^2 b_2} = ... = p_K + \frac{\sigma^2}{|\beta_K|^2 b_K}. \tag{34}$$

From (34), it is found that the power is approximately equal for smaller σ^2. Let $P = \sum_{k=1}^{K} p_k$ and $\zeta_k = |\beta_k|^2 b_k / \sigma^2$, then with (34), we can obtain:

$$p_k = \frac{P}{K} + \frac{1}{K} \sum\nolimits_{i=1}^{K} \frac{1}{\zeta_i} - \frac{1}{\zeta_k}. \tag{35}$$

Substituting (35) into the objective function in (29) yields

$$J_7 = \frac{\sum_{k=1}^{K} \log(\frac{P \zeta_k}{K} + \frac{\zeta_k}{K} \sum_{i=1}^{K} \frac{1}{\zeta_i})}{(\varrho P + P_c) \log 2}. \tag{36}$$

Hence, using (36), the original problem (29) is transformed into the optimization problem w.r.t. P, i.e,

$$\begin{aligned} &\max_{P} J_{10} = \frac{\log(P + \sum_{i=1}^{K} \frac{1}{\zeta_i}) + \frac{1}{K} \sum_{k=1}^{K} \log(\zeta_k) - \log(K)}{(\varrho P + P_c) \log 2} \\ &\text{s.t.} \quad P \leq P_{max}, \end{aligned} \tag{37}$$

With (37), we can calculate $\partial J_{10} / \partial P$ as

$$\frac{\partial J_{10}}{\partial P} = \frac{\frac{\varrho P + P_c}{P + \sum_{i=1}^{K} \zeta_i^{-1}} - \varrho \log(P + \sum_{i=1}^{K} \zeta_i^{-1}) - \varrho \Psi}{(\varrho P + P_c)^2 \log 2}, \tag{38}$$

where $\Psi = \frac{1}{K} \sum_{k=1}^{K} \log(\zeta_k) - \log(K)$. By setting $\partial J_{10} / \partial P$=0 and using the Lambert W function [38], P can be attained as

$$P^o = \exp\{W(e^{\Psi - 1}(\varrho^{-1} P_c - \sum\nolimits_{i=1}^{K} \zeta_i^{-1})) + 1 - \Psi\}. \tag{39}$$

Considering the maximum power constraint, the optimal P can be rewritten as $P^* = \min(P^o, P_{max})$. Substituting this into (35) gives

$$p_k = \frac{P^*}{K} + \frac{1}{K} \sum\nolimits_{i=1}^{K} \frac{1}{\zeta_i} - \frac{1}{\zeta_k}. \tag{40}$$

From (40), we can find that when ζ_k is small, p_k is also small. Thus, for the users with small p_k, their rate may not meet the requirement of r_0. Based on this, we can set these users' rate equal to r_0 to obtain the corresponding PA. Hence, by sorting ζ_k in descending order (i.e., $\zeta_1 > ... > \zeta_K$), the $\{p_k\}$ can be re-expressed as

$$\begin{aligned} &p_k = \frac{P^* - \sum_{i=K_0+1}^{K} \rho_0 \zeta_i^{-1}}{K_0} + \frac{1}{K_0} \sum\nolimits_{i=1}^{K_0} \frac{1}{\zeta_i} - \frac{1}{\zeta_k}, k = 1, ..., K_0, \\ &\text{and} \;\; p_k = \rho_0 / \zeta_k, \qquad\qquad k = K_0 + 1, ..., K, \end{aligned} \tag{41}$$

where K_0 can be determined by the following procedure. Let $U_n = \sum_{i=1}^{n} \zeta_i^{-1}$ and $V_n = \sum_{i=n+1}^{K} \rho_0 \zeta_i^{-1}$. Starting from $n = K$, compute $p_n(\zeta_n) = \frac{P^* - V_n}{n} + \frac{U_n}{n} - \frac{1}{\zeta_n}$. If $p_n(\zeta_n) \geq \rho_0 \zeta_n^{-1}$,

This article has been accepted for publication in a future issue of this journal, but has not been fully edited. Content may change prior to final publication. Citation information: DOI10.1109/JSAC.2022.3196111 IEEE Journal on Selected Areas in Communications

then $K_0 = n$, otherwise, compute $U_{n-1} = U_n - \zeta_n^{-1}$ and $V_{n-1} = V_n + \rho_0\zeta_n^{-1}$, set $n = n-1$, and repeat the calculation of $p_n(\zeta_n)$ until it is not less than $\rho_0\zeta_n^{-1}$.

Given the beam gain $\mathbf{b}$, position $\{x_0, y_0\}$ and PA $\mathbf{p}$, the BCD method is employed to update their values iteratively until the algorithm converges. As a result, the optimized beam gain coefficients, position and PA coefficients are respectively attained. This joint design scheme for position optimization is referred as joint-scheme1 for ease of presentation. The specific procedure is summarized in Algorithm 1

Algorithm 1 Joint design algorithm for joint-scheme1

1: **Initialize**: Tolerance $\epsilon > 0$, iteration index i=0, initial value $\{\mathbf{p}^{(0)}, (x_0^{(0)}, y_0^{(0)})\}$
2: Compute $\eta_{EE}^{(0)}$ by (7);
3: **repeat**
4: $i = i + 1$;
5: Update $\mathbf{b}^{(i)}$ for fixed $\mathbf{p}^{(i-1)}$ and $(x_0^{(i-1)}, y_0^{(i-1)})$ according to (15);
6: Update $(x_0^{(i)}, y_0^{(i)})$ for fixed $\mathbf{b}^{(i)}$ and $\mathbf{p}^{(i-1)}$ according to (24) or (27);
7: Update $\mathbf{p}^{(i)}$ for fixed $\mathbf{b}^{(i)}$ and $(x_0^{(i)}, y_0^{(i)})$ according to (41);
8: Compute $\eta_{EE}^{(i)}$ by (7);
9: **until** $|\eta_{EE}^{(i)} - \eta_{EE}^{(i-1)}| < \epsilon$
10: **Output**: Suboptimal solution $\{\mathbf{b}^{(i)}, \mathbf{p}^{(i)}, (x_0^{(i)}, y_0^{(i)})\}$.

IV. Joint Optimization Design of BF and PA

In this section, we give the joint design of beamforming and PA for maximizing EE, based on the UAV position attained by Algorithm 1.

A. BF design given PA

Given the UAV position, the original problem (8) is simplified as

$$\begin{aligned} \max_{\mathbf{p},\mathbf{w}} J_1 = & \frac{\sum_{k=1}^{K} \log_2(1 + p_k|\mathbf{h}_k^H\mathbf{w}|^2/\sigma^2)}{\varrho\sum_{k=1}^{K} p_k + P_c} \\ \text{s.t. } & C_1, C_2, C_3. \end{aligned} \tag{42}$$

Given the PA $\mathbf{p}$ (the initial $\mathbf{p}$ may be from Algorithm 1), the above problem can be simplified as the optimization of $\mathbf{w}$ only, i.e.,

$$\begin{aligned} \max_{\mathbf{w}} J_{11} = & \sum\nolimits_{k=1}^{K} \log_2(1 + p_k|\mathbf{h}_k^H\mathbf{w}|^2/\sigma^2) \\ \text{s.t. } & C_2, C_3. \end{aligned} \tag{43}$$

Then, we transform the problem (43) into:

$$\begin{aligned} \max_{\mathbf{w},\{z_k\}} J_{12} = & \sum\nolimits_{k=1}^{K} \log_2(1 + p_k z_k^2/\sigma^2) \\ \text{s.t. } & C_7 : z_k = |\mathbf{h}_k^H\mathbf{w}| \\ & C_8 : z_k \geq (\rho_0\sigma^2/p_k)^{1/2}, C_3. \end{aligned} \tag{44}$$

Given the $\mathbf{w}$, problem (44) is simplified as the one w.r.t. z_k only. Under this case, the objective function in (44) is concave w.r.t. z_k (considering σ^2 is smaller in general), and the constraints are linear, therefore the problem (44) is convex. Thus, it has the optimal solution. In order to tackle the equality constraint, we employ the penalty function method in [39] to add a quadratic penalty term into the objective function of (44), which yields the following optimization problem:

$$\begin{aligned} \max_{\{z_k\}} J_{13} = & \sum\nolimits_{k=1}^{K} \log(1 + p_k z_k^2/\sigma^2) \\ & - \frac{1}{2}\varsigma^{(u-1)} \sum\nolimits_{k=1}^{K} (z_k - |\mathbf{h}_k^H\mathbf{w}|)^2 \\ \text{s.t. } & C_8, \end{aligned} \tag{45}$$

where $\varsigma^{(u-1)}$ is the penalty variable of the $u-1$ iteration, which is updated by $\varsigma^{(u)} = \tau\varsigma^{(u-1)} (\tau > 1)$.

Let $\delta_k = |\mathbf{h}_k^H\mathbf{w}|$, then with (45), we can calculate $\partial J_{13}/\partial z_k$ as

$$\frac{\partial J_{13}}{\partial z_k} = \frac{2p_k z_k}{\sigma^2 + p_k z_k^2} - \varsigma(z_k - \delta_k), \tag{46}$$

where ς^{u-1} is simplified as ς for convenient calculation. By setting $\partial J_{13}/\partial z_k = 0$, we have:

$$p_k z_k^3 - \delta_k p_k z_k^2 + (\sigma^2 - 2p_k\varsigma^{-1})z_k - \delta_k\sigma^2 = 0. \tag{47}$$

It is a cubic equation w.r.t. z_k. For a cubic equation shown as (48), it has three solutions.

$$At^3 + Bt^2 + Ct + D = 0 \quad (t \geq 0)\,. \tag{48}$$

This equation can be solved by the Cardan formula, and corresponding three solutions are given by

$$\begin{aligned} t_1 &= \Phi + \Psi - B/(3A), \\ t_2 &= \nu\Phi + \nu^2\Psi - B/(3A), \\ t_3 &= \nu^2\Phi + \nu\Psi - B/(3A), \end{aligned} \tag{49}$$

where $\tau = \frac{3AC-B^2}{3A^2}$, $\mu = \frac{27A^2D-9ABC+2B^3}{27A^3}$, $\nu = \frac{-1+\sqrt{3}i}{2}$, $\Xi = \sqrt{(\frac{\mu}{2})^2 + (\frac{\tau}{3})^3}$, $\Phi = \sqrt[3]{-\frac{\mu}{2} + \Xi}$, and $\Psi = \sqrt[3]{-\frac{\mu}{2} - \Xi}$.

Lemma 1: Equation (48) has one or three positive real-valued solution when $A > 0$ and $D < 0$.

Proof: Please see Appendix B. ■

Because $A = p_k > 0$ and $D = -\delta_k\sigma^2 < 0$, equation (47) has one or three positive real-valued solutions. Considering the noise power σ^2 is smaller in general, $C = \sigma^2 - 2p_k\varsigma^{-1}$ will be smaller than zero. Thus, (47) has one positive real-valued solution, z_k^*. If (47) has three positive real-valued solutions, the biggest one is z_k^* as we need it to maximize the objective function and meet the requirement of r_0. Due to the constraint of C_8, for $z_k < z_k^0$, z_k is updated as $z_k^* = z_k^0$, where $z_k^0 = (\rho_0\sigma^2 p_k^{-1})^{1/2}$ is from C_8.

With the obtained z_k, we update the $\mathbf{w}$, and corresponding subproblem w.r.t $\mathbf{w}$ is formulated as

$$\begin{aligned} \min_{\mathbf{w}} J_{14} = & \sum\nolimits_{k=1}^{K} (z_k - |\mathbf{h}_k^H\mathbf{w}|)^2 \\ \text{s.t. } & C_3 : |[\mathbf{w}]|_m = 1/\sqrt{M}, m = 1, ...M. \end{aligned} \tag{50}$$

Since $\sum_{k=1}^{K} (z_k - |\mathbf{h}_k^H\mathbf{w}|)^2 = \sum_{k=1}^{K} z_k^2 - 2z_k|\mathbf{h}_k^H\mathbf{w}| + |\mathbf{h}_k^H\mathbf{w}|^2$, and z_k is known, the problem J_{14} is equivalent to

$$\begin{aligned} \min_{\mathbf{w}} \ & J_{15} = \sum\nolimits_{k=1}^{K} |\mathbf{h}_k^H\mathbf{w}|^2 - 2z_k|\mathbf{h}_k^H\mathbf{w}| \\ \text{s.t. } & C_3 \end{aligned} \tag{51}$$

Utilizing the inequality $|a||b| \geq \text{Re}\{ab^*\}$, then we have: $|\mathbf{h}_k^H\mathbf{w}||\mathbf{h}_k^H\mathbf{w}^{(r-1)}| \geq \text{Re}\{\mathbf{h}_k^H\mathbf{w}\mathbf{w}^{(r-1)H}\mathbf{h}_k\}$ [40],

This article has been accepted for publication in a future issue of this journal, but has not been fully edited. Content may change prior to final publication. Citation information: DOI10.1109/JSAC.2022.3196111 IEEE Journal on Selected Areas in Communications

where $\mathbf{w}^{(r-1)}$ is $(r-1)$-th iteration of $\mathbf{w}$. Thus, $|\mathbf{h}_k^H\mathbf{w}| \geq \mathrm{Re}\{\mathbf{h}_k^H\mathbf{w}\mathbf{w}^{(r-1)H}\mathbf{h}_k\}/|\mathbf{h}_k^H\mathbf{w}^{(r-1)}|$. With this result, the convex majorization problem for (51) is given by

$$\begin{aligned}\min_{\mathbf{w}} J_{16} &= \sum\nolimits_{k=1}^{K} |q_k - \mathbf{h}_k^H\mathbf{w}|^2 \\ &= \mathbf{w}^H\mathbf{F}\mathbf{w} - 2\,\mathrm{Re}\{\mathbf{w}^H\mathbf{f}\} + \sum\nolimits_{k=1}^{K} |q_k|^2, \\ \text{s.t.} \quad & C_3,\end{aligned} \tag{52}$$

where $q_k = z_k\mathbf{h}_k^H\mathbf{w}^{(r-1)}/|\mathbf{h}_k^H\mathbf{w}^{(r-1)}|$, $\mathbf{F} = \sum_{k=1}^{K}\mathbf{h}_k\mathbf{h}_k^H$, and $\mathbf{f} = \sum_{k=1}^{K}\mathbf{h}_k q_k$.

The tight upper bound of $\mathbf{w}^H\mathbf{F}\mathbf{w}$ at r-th iteration in Majorization-Minimization (MM) algorithm [40] is given by

$$\mathbf{w}^H\mathbf{F}\mathbf{w} \leqslant \mathbf{w}^H\tilde{\mathbf{F}}\mathbf{w} - 2\,\mathrm{Re}\left\{\mathbf{w}^H\mathbf{v}^{(r-1)}\right\} + \mathbf{w}^{(r-1)H}\mathbf{v}^{(r-1)} \tag{53}$$

where $\mathbf{v}^{(r-1)} = (\tilde{\mathbf{F}} - \mathbf{F})\mathbf{w}^{(r-1)}$, $\tilde{\mathbf{F}} = \lambda_{\max}(\mathbf{F})\mathbf{I}_M$, and $\lambda_{\max}(\mathbf{F})$ is the maximum eigenvalue of $\mathbf{F}$, and is from the eigenvalue decomposition (EVD) of $\mathbf{F}$. For the feasible solution $\mathbf{w}$ in (52), $\mathbf{w}^{\mathrm{H}}\tilde{\mathbf{F}}\mathbf{w} = \lambda_{\max}(\mathbf{F})$ is a constant.

Discarding the constants independent of $\mathbf{w}$, problem (52) is approximated as

$$\begin{aligned}\max_{\mathbf{w}} \quad & J_{17} = \mathrm{Re}\{\mathbf{w}^H\tilde{\mathbf{v}}^{(r-1)}\} \\ \text{s.t.} \quad & C_3,\end{aligned} \tag{54}$$

where $\tilde{\mathbf{v}}^{(r-1)} = \mathbf{v}^{(r-1)} + \mathbf{f}$. Then problem (54) can be divided into M subproblem as

$$\begin{aligned}\max_{\psi_m} \quad & J_{18} = \cos\left(\varphi_m^{(r-1)} - \psi_m\right) \\ \text{s.t.} \quad & 0 \leqslant \psi_m \leqslant 2\pi,\end{aligned} \tag{55}$$

where $\varphi_m^{(r-1)}$ and ψ_m are the phases of $(\tilde{\mathbf{v}}^{(r-1)})_m$ and $(\mathbf{w})_m$, respectively. Obviously, the optimal solution of (55) is $\psi_m^o = \varphi_m^{(r-1)}$. Thus, the optimal solution of (54) is

$$\mathbf{w}^o = \frac{1}{\sqrt{M}}[\exp(j\psi_1^o), ..., \exp(j\psi_M^o)]^T \tag{56}$$

Based on the obtained $\mathbf{w}^o$ and $\{z_k\}$, the BCD method is exploited to update their values iteratively until they converge. As a result, the near-optimal $\mathbf{w}^o$ and $\{z_k\}$ are achieved, respectively for the given PA. Correspondingly, the algorithm realization for solving problem (44) is illustrated as Algorithm 2, and this BF scheme is referred as sub-BF1 for easy presentation.

$$\begin{aligned}\Gamma^{(r)} &= \sum\nolimits_{k=1}^{K} \log_2\left(1 + p_k\big(z_k^{(r)}\big)^2/\sigma^2\right) \\ &\quad - \frac{1}{2}\varsigma^{(u-1)}\sum\nolimits_{k=1}^{K} \left(z_k^{(r)} - |\mathbf{h}_k^H\mathbf{w}^{(r)}|\right)^2\end{aligned} \tag{57}$$

$$\Xi^{(r)} = \max_{k\in\{1,...K\}} \left\{\left|z_k^{(r)} - |\mathbf{h}_k^H\mathbf{w}^{(r)}|\right|\right\}, \tag{58}$$

where $z_k^{(r)}$ is the r-th iteration of z_k.

Algorithm 2 Algorithm for solving subproblem (44)

1: **Initialize**: Tolerance $\epsilon_1 > 0$, iteration index u=0, inter tolerance $\epsilon_2 > 0$, inter iteration index r, penalty parameters $\{\varsigma^{(0)} > 0, \tau > 1\}$, constraint violation $\Xi^{(0)} = +\infty$;
2: **repeat**
3: $u = u + 1$;
4: initial point $\{\mathbf{w}^{(0)}, \mathbf{z}^{(0)}\}$, the value of objective function $\Gamma^{(0)} = 0$, and $r = 0$;
5: **repeat**
6: $r = r + 1$;
7: Update $\mathbf{z}^{(r)}$ for fixed $\{\mathbf{w}^{(r-1)}\}$ according to (47)-(49);
8: Update $\mathbf{w}^{(r)}$ for fixed $\{\mathbf{z}^{(r)}\}$ according to (56);
9: Calculate $\Gamma^{(r)}$ according to (57);
10: **until** $\left|\Gamma^{(r)} - \Gamma^{(r-1)}\right| < \epsilon_2$
11: Calculate $\Xi^{(r)}$ according to (58);
12: **if** $\Xi^{(r)} \leq \epsilon_1$ **then**
13: **flag** $= 1$;
14: **else**
15: $\varsigma^{(u)} = \tau\varsigma^{(u-1)}$;
16: **end if**
17: **until flag** $= 1$
18: **Output**: A suboptimal solution $\{\mathbf{w}^{(r)}, \mathbf{z}^{(r)}\}$ for (44).

B. PA design given BF

Using the obtained BF $\mathbf{w}^o$ above, we give the PA optimization in this subsection. Under this case, the optimization problem (42) is simplified as

$$\begin{aligned}\max_{\mathbf{p}} J_{19} &= \frac{\sum_{k=1}^{K}\log_2(1 + p_k|\mathbf{h}_k^H\mathbf{w}^o|^2/\sigma^2)}{\varrho\sum_{k=1}^{K}p_k + P_c} \\ \text{s.t.} \; & C_1, C_2.\end{aligned} \tag{59}$$

For the problem (59), we can adopt the calculation method in section III-C to obtain the optimal PA, i.e, the $\{p_k\}$ shown as (41), where ζ_k is changed to $\zeta_k = |\mathbf{h}_k^H\mathbf{w}^o|^2/\sigma^2$.

Based on the obtained BF vector and PA coefficients, using the BCD method, we can finally achieve the optimized BF and PA by iterative calculation. This joint design scheme is referred as joint-scheme2 for ease of presentation, and correspondingly, the algorithm procedure is summarized as Algorithm 3.

Algorithm 3 Joint BF and PA algorithm for joint-scheme2

1: **Initialize**: Initial point $\{\mathbf{p}^{(0)}, \mathbf{w}^{(0)}\}$, tolerance $\epsilon > 0$, iteration index $l = 0$, (x_0^*, y_0^*) given by Algorithm 1;
2: Compute $\eta_{EE}^{(0)}$ by (7);
3: **repeat**
4: $l = l + 1$;
5: Update $\mathbf{w}^{(l)}$ for fixed $\{\mathbf{p}^{(l-1)}\}$ according to Algorithm 2;
6: Update $\mathbf{p}^{(l)}$ for fixed $\{\mathbf{w}^{(l)}\}$ according to (41) with $\zeta_k = |\mathbf{h}_k^H\mathbf{w}^{(l)}|^2/\sigma^2$;
7: Compute $\eta_{EE}^{(l)}$ by (7);
8: **until** $|\eta_{EE}^{(l)} - \eta_{EE}^{(l-1)}| < \epsilon$
9: **Output**: Suboptimal solution $\{\mathbf{w}^{(l)}, \mathbf{p}^{(l)}\}$.

C. Suboptimal BF with low complexity

It is found that the proposed Algorithm 3 needs three-loop iteration, where BF design needs two-loop iteration (see Algorithm 2), and the complexity may be high. For this reason, in this subsection, we will give two suboptimal BF designs to lower the complexity.

Since the beam gain $\{b_k\}$ is given by the Algorithm 1, we can exploit it to design low-complexity suboptimal BF. Let $e_k = |\beta|_k^2 b_k$, then $e_k \approx |\mathbf{h}_k^H \mathbf{w}|^2$ in terms of (9). By minimizing $\sum_{k=1}^{K}(|\mathbf{h}_k^H \mathbf{w}| - \sqrt{e_k})^2$ subject to C_3, shown as (60), the suboptimal BF can be attained.

$$\begin{aligned}&\min_{\mathbf{w}} J_{20} = \sum\nolimits_{k=1}^{K} (|\mathbf{h}_k^H \mathbf{w}| - \sqrt{e_k})^2 \\ &\text{s.t.} \quad C_3.\end{aligned} \tag{60}$$

Using the derivation method shown in (50)-(56) and MM algorithm, the suboptimal $\mathbf{w}$ is obtained as

$$\tilde{\mathbf{w}}^o = \frac{1}{\sqrt{M}} \left[\exp(j\tilde{\psi}_1^o), ..., \exp(j\tilde{\psi}_M^o)\right]^T, \tag{61}$$

where $\tilde{\psi}_m^o = \tilde{\varphi}_m^{(r-1)}$, $\tilde{\varphi}_m^{(r-1)}$ is the phases of $(\breve{\mathbf{v}}^{(r-1)})_m$, and $\breve{\mathbf{v}}^{(r-1)}$ is

$$\breve{\mathbf{v}}^{(r-1)} = \mathbf{v}^{(r-1)} + \tilde{\mathbf{f}} = (\tilde{\mathbf{F}} - \mathbf{F})\mathbf{w}^{(r-1)} + \sum\nolimits_{k=1}^{K} \mathbf{h}_k c_k, \tag{62}$$

where $c_k = \sqrt{e_k}\mathbf{h}_k^H \mathbf{w}^{(r-1)}/|\mathbf{h}_k^H \mathbf{w}^{(r-1)}|$.

Based on the (61) and (62), utilizing the iterative calculation, the final optimized BF can be obtained. This BF scheme is referred as sub-BF2 for easy presentation. Due to single-layer iteration and the closed-form solution for each iteration, this suboptimal BF2 has lower complexity than the suboptimal BF1, and only small performance loss is found. After obtaining $\tilde{\mathbf{w}}^o$, following the method in Section III-C, the PA $\{b_k\}$ can be recalculated once to meet the rate requirement. Correspondingly, the algorithm realization is shown as Algorithm 4, and this joint scheme is referred as joint-scheme3.

Algorithm 4 Algorithm design for joint-scheme3

1: **Initialize**: Initial point $\tilde{\mathbf{w}}^{(0)}$, tolerance $\epsilon > 0$, iteration index $r = 0$, $\mathbf{b}$, (x_0^*, y_0^*) and initial $\mathbf{p}$ are from Algorithm 1;
2: **repeat**
3: $r = r + 1$;
4: Update $[\tilde{\mathbf{w}}^{(r)}]$ according to (61);
5: **until** $||\tilde{\mathbf{w}}^{(r)} - \tilde{\mathbf{w}}^{(r-1)}|| < \epsilon$;
6: Compute $\mathbf{p}$ by (41) with $\zeta_k = |\mathbf{h}_k^H \tilde{\mathbf{w}}^{(r)}|^2/\sigma^2$;
7: **Output**: Suboptimal solution $\{\tilde{\mathbf{w}}^{(r)}, \mathbf{p}\}$.

Considering that the above suboptimal BF2 still needs iteration, in the following, we present another low-complexity BF design with closed-form solution. Based on the obtained PA in Algorithm 1, the objective function in (43) is lower bounded by $\sum_{k=1}^{K}\log_2(1 + p_k|\mathbf{h}_k^H \mathbf{w}|^2/\sigma^2) \geq \log_2(1 + \sum_{k=1}^{K} p_k|\mathbf{h}_k^H \mathbf{w}|^2/\sigma^2)$. By maximizing this lower bound, a suboptimal BF is attained. Based on this, the problem (43) becomes

$$\begin{aligned}&\max_{\mathbf{w}} J_{19} = \log_2(1 + \sum\nolimits_{k=1}^{K} p_k|\mathbf{h}_k^H \mathbf{w}|^2/\sigma^2) \\ &\text{s.t. } C_2, C_3.\end{aligned} \tag{63}$$

The problem (63) is equivalent to

$$\begin{aligned}&\max_{\mathbf{w}} J_{20} = \frac{\sum_{k=1}^{K} p_k|\mathbf{h}_k^H \mathbf{w}|^2}{\sigma^2} = \frac{\mathbf{w}^H(\sum_{k=1}^{K} p_k \mathbf{h}_k \mathbf{h}_k^H)\mathbf{w}}{\sigma^2} \\ &\text{s.t. } C_2, C_3.\end{aligned} \tag{64}$$

The objective function J_{20} can be maximized by using the EVD, and the corresponding optimal $\mathbf{w}$ is expressed as $\hat{\mathbf{w}}^o = \vec{\lambda}_{\max}\left(\sum_{k=1}^{K} p_k \mathbf{h}_k \mathbf{h}_k^H\right)$. Considering C_3 constraint, the elements of the BF vector after CM normalization are given by

$$[\hat{\mathbf{w}}^*]_m = \frac{[\hat{\mathbf{w}}^o]_m}{\sqrt{M}|[\hat{\mathbf{w}}^o]|_m} \tag{65}$$

Thus, the BF $\hat{\mathbf{w}}^*$ satisfies the CM constraint. Moreover, the closed-form suboptimal BF is attained. This BF scheme is referred as sub-BF3, and it has lower complexity than the above suboptimal BF1 and suboptimal BF2 because of closed-form solution. For single user (K=1), $\hat{\mathbf{w}}^o$ is optimal solution for problem (43). Therefore, this sub-BF3 is more suitable for a few number of users. Based on the obtained $\hat{\mathbf{w}}^*$, using the calculation method in Algorithm 1, the PA $\{b_k\}$ is recalculated once to meet the minimal rate requirement. Specifical algorithm procedure is illustrated as Algorithm 5, and correspondingly, this joint scheme is referred as joint-scheme4. Besides, $\hat{\mathbf{w}}^*$ can also be used for the initial value of $\mathbf{w}$ in Algorithms 3 and 4 to reduce the iteration.

Algorithm 5 Algorithm design for joint-scheme4

1: **Initialize**: Initial $\mathbf{p}$ and (x_0^*, y_0^*) given by Algorithm 1;
2: Calculate $\hat{\mathbf{w}}$ by (65) with EVD;
3: Compute $\mathbf{p}$ by (41) with $\zeta_k = |\mathbf{h}_k^H \hat{\mathbf{w}}|^2/\sigma^2$;
4: **Output**: Suboptimal solution $\{\hat{\mathbf{w}}, \mathbf{p}\}$.

V. Special cases

In this subsection, we give the joint optimization of BF, PA and position under two special cases, where one is that only LoS component exists, and the other is that only NLoS component exists. For these two cases, we do not need to perform two-step optimization above, and can joint optimize the BF, PA and position directly.

For the first case, according to (4), we have:

$$|\mathbf{w}^H \mathbf{h}_k^{Los}|^2 = (\lambda_0/(4\pi))^2 d_k^{-\alpha_{Los}} |\mathbf{w}^H \mathbf{a}(M, \theta_{k,0})|^2, \tag{66}$$

and for the second case, we have:

$$\begin{aligned}|\mathbf{w}^H \mathbf{h}_k^{Nlos}|^2 &= (\lambda_0/(4\pi))^2 d_k^{-\alpha_{NloS}} \\ &\times |\mathbf{w}^H \sum\nolimits_{l=1}^{L_k} \xi_{k,l}\mathbf{a}(M, \theta_{k,l})/\sqrt{L_k}|^2.\end{aligned} \tag{67}$$

Thus, with (66) and (67), we can obtain:

$$|\mathbf{w}^H \mathbf{h}_k|^2 = \tilde{c} d_k^{-\alpha} \tilde{b}_k, \tag{68}$$

where $\tilde{c}$=$(\lambda_0/(4\pi))^2$, α=α_{Nlos} and $\tilde{b}_k$=$|\mathbf{w}^H \sum_{l=1}^{L_k} \xi_{k,l}\mathbf{a}(M, \theta_{k,l})/\sqrt{L_k}|^2$ for the second case, α=α_{Los} and $\tilde{b}_k$=$|\mathbf{w}^H \mathbf{a}(M, \theta_{k,0})|^2$ for the first case.

In what follows, with (8) and (68), we provide the joint optimization of BF, PA and UAV position.

Firstly, we perform the optimization of BF given PA $\{p_k\}$ and position $\{x_o, y_o\}$. Under this case, we use the method in Section IV-A (i.e., suboptimal BF1 scheme) to obtain near optimal BF $\mathbf{w}^o$. Secondly, with the obtained BF and the given PA, we optimize the UAV position. Under this case, by substituting (68) into (8), one can then employ the method

This article has been accepted for publication in a future issue of this journal, but has not been fully edited. Content may change prior to final publication. Citation information: DOI10.1109/JSAC.2022.3196111 IEEE Journal on Selected Areas in Communications

in Section III-B to achieve the suboptimal position $\{x_o^*, y_o^*\}$. Thirdly, based on the obtained BF and UAV position, we optimize the PA. For this case, we can use the method in Section III-C to obtain the optimal PA coefficients $\{p_k\}$, shown as (41) with $\zeta_k = |\mathbf{h}_k^H \mathbf{w}^o|^2/\sigma^2$. Finally, with the obtained BF $\mathbf{w}$, position $\{x_o, y_o\}$ and PA $\{p_k\}$, the BCD method is employed to update their values iteratively until the algorithm converges. As a result, the optimized BF, position and PA coefficients are respectively attained. Correspondingly, the joint design scheme (which is referred as joint-scheme5) is presented, and the algorithm realization is summarized in Algorithm 6.

Algorithm 6 Joint design algorithm of BF, position and PA for special cases

1: **Initialize**: Tolerance $\epsilon > 0$, iteration index i=0, initial value $\{\mathbf{p}^{(0)}, \mathbf{w}^{(0)}, (x_0^{(0)}, y_0^{(0)})\}$
2: Compute $\eta_{EE}^{(0)}$ by (7);
3: **repeat**
4: $i = i + 1$;
5: Update $\mathbf{w}^{(i)}$ for fixed $\{\mathbf{p}^{(i-1)}\}$ and $(x_0^{(i-1)}, y_0^{(i-1)})$ according to Algorithm 2;
6: Update $(x_0^{(i)}, y_0^{(i)})$ for fixed $\mathbf{w}^{(i)}$ and $\mathbf{p}^{(i-1)}$ according to (24) or (27) by means of (68);
7: Update $\mathbf{p}^{(i)}$ for fixed $\mathbf{w}^{(i)}$ and $(x_0^{(i)}, y_0^{(i)})$ according to (41) with $\zeta_k = |\mathbf{h}_k^H \mathbf{w}^{(i)}|^2/\sigma^2$;
8: Compute $\eta_{EE}^{(i)}$ by (7);
9: **until** $|\eta_{EE}^{(i)} - \eta_{EE}^{(i-1)}| < \epsilon$
10: **Output**: Suboptimal solution $\{\mathbf{w}^{(i)}, \mathbf{p}^{(i)}, (x_0^{(i)}, y_0^{(i)})\}$.

Besides, considering that the used suboptimal BF1 scheme needs two-loop iteration, we can use the suboptimal BF3 to replace the suboptimal BF1 for BF design. Correspondingly, the closed-form BF is obtained under the given PA and position. Thus, the complexity is greatly reduced.

VI. Complexity and Convergence Analysis

In this section, we firstly give the complexity analysis of the proposed algorithms. Regarding the Algorithm 1, it mainly involves the iteration of BCD method. For each iteration, K beam gains and PA coefficients as well as a pair of coordinates need to be computed. Therefore, the complexity is approximated as $\mathcal{O}\left(I_1^{(1)}(2K + 2I_1^{(2)})\right)$, where $I_1^{(1)}$ is the iterative number of BCD, $I_1^{(2)}$ is iterative number of the fixed point iteration method (for the position) and is small, which equals one for α=2 (without iteration). In Algorithm 3, except including the complexity of Algorithm 1, the main calculation also involves three-loop iterations, EVD and matrix multiplication. Hence, the complexity is approximated as $\mathcal{O}\left((M^3 + KM^2 + M^2 + K)I_2^{(2)} I_2^{(3)} + K)I_2^{(1)}\right)$ plus the complexity of Algorithm 1, where $I_2^{(1)}$ is number of the outer iteration of BCD, $I_2^{(2)}$ is the number of inner iteration of penalty function method, and $I_2^{(3)}$ is the number of innermost iteration of BCD. Algorithm 4 mainly involves one-loop iteration, EVD and matrix multiplication, and corresponding complexity is approximated as $\mathcal{O}\left((M^3 + KM^2 + M^2)I_3 + K\right)$ plus the complexity of Algorithm 1, where I_3 is the iterative number of MM algorithm. Algorithm 5 mainly involves EVD and matrix multiplication, and corresponding complexity is approximated as $\mathcal{O}\left(M^3 + KM^2 + M + K\right)$ plus the complexity of Algorithm 1. Hence, Algorithm 5 has lower complexity than Algorithms 3 and 4, and Algorithm 4 also has lower complexity than Algorithm 3. Besides, Algorithm 6 mainly involves three-loop iterations, EVD and matrix multiplication. Hence, the complexity is approximated as $\mathcal{O}\left((M^3 + KM^2 + M^2 + K)I_6^{(2)} I_6^{(3)} + K + 2I_6^{(4)})I_6^{(1)}\right)$, $I_6^{(1)}$ is number of the outer iteration of BCD, $I_6^{(2)}$ is the number of inner iteration of penalty function method, $I_6^{(3)}$ is the number of innermost iteration of BCD, and $I_6^{(4)}$ is the number of inner iteration of the fixed point iteration method, and it is one for α=2.

In what follows, we will analyze the convergence of Algorithm 1 and Algorithm 3. Firstly, Algorithm 1 is considered. We divide the original problem (10) into three subproblems and optimize the beam gain $\mathbf{b}$, UAV position Θ=$\{x_0, y_0\}$ and PA $\mathbf{p}$ alternately by solving the subproblems (11), (16) and (29). For easy analysis, we define $f(\mathbf{b}, \Theta, \mathbf{p})$ as the objective function of optimization variables $\mathbf{b}, \Theta, \mathbf{p}$.

In step (5) of Algorithm 1, with given variables $\Theta^{(r-1)}$, $\mathbf{p}^{(r-1)}$, we can obtain the optimal $\mathbf{b}^{(r)}$ by solving problem (11). Thus, we have:

$$f(\mathbf{b}^{(r)}, \Theta^{(r-1)}, \mathbf{p}^{(r-1)}) \geq f(\mathbf{b}^{(r-1)}, \Theta^{(r-1)}, \mathbf{p}^{(r-1)}), \tag{69}$$

where r is the iterative index.

In step (6) of Algorithm 1, with given variables $\mathbf{b}^{(r)}$, $\mathbf{p}^{(r-1)}$, we can obtain the optimal $\Theta^{(r)}$ by solving problem (20). Thus, it guarantees that

$$f(\mathbf{b}^{(r)}, \Theta^{(r)}, \mathbf{p}^{(r-1)}) \geq f(\mathbf{b}^{(r)}, \Theta^{(r-1)}, \mathbf{p}^{(r-1)}), \tag{70}$$

In step (7) of Algorithm 1, with given variables $\mathbf{b}^{(r)}$, $\Theta^{(r)}$, we can obtain the optimal $\mathbf{p}^{(r)}$ by solving problem (29). Thus, it follows that

$$f(\mathbf{b}^{(r)}, \Theta^{(r)}, \mathbf{p}^{(r)}) \geq f(\mathbf{b}^{(r)}, \Theta^{(r)}, \mathbf{p}^{(r-1)}), \tag{71}$$

Substituting (69) and (70) into (71) yields

$$f(\mathbf{b}^{(r)}, \Theta^{(r)}, \mathbf{p}^{(r)}) \geq f(\mathbf{b}^{(r-1)}, \Theta^{(r-1)}, \mathbf{p}^{(r-1)}), \tag{72}$$

The above results indicate that the objective value is increasing after each iteration. Moreover, because of the limited power, the sum rate is also limited. Thus, the EE (i.e., objective value) is upper-bounded. Hence, the proposed Algorithm 1 can be guaranteed to converge.

Similarly, we can analyze the convergence of Algorithm 3. Namely, based on the analytical method above, we can obtain:

$$\begin{aligned} &\Upsilon_1 : f(\mathbf{w}^{(l)}, \mathbf{p}^{(l-1)}) \geq f(\mathbf{w}^{(l-1)}, \mathbf{p}^{(l-1)}), \\ &\Upsilon_2 : f(\mathbf{w}^{(l)}, \mathbf{p}^{(l)}) \geq f(\mathbf{w}^{(l)}, \mathbf{p}^{(l-1)}) \end{aligned} \tag{73}$$

where l is iterative index, Υ_1 holds due to the iterative convergence of Algorithm 2, and Υ_2 holds because the obtained $\mathbf{p}^{(l)}$ is the optimal solution of the problem (59). With (73), we have:

$$f(\mathbf{w}^{(l)}, \mathbf{p}^{(l)}) \geq f(\mathbf{w}^{(l-1)}, \mathbf{p}^{(l-1)}), \tag{74}$$

This article has been accepted for publication in a future issue of this journal, but has not been fully edited. Content may change prior to final publication. Citation information: DOI10.1109/JSAC.2022.3196111 IEEE Journal on Selected Areas in Communications

The above results show that the objective value is increasing after each iteration. Moreover, the objective function of the problem (42) is also upper-bounded due to the limited power. As a result, the proposed Algorithm 3 can be guaranteed to converge.

VII. Simulation Results

In this section, we evaluate the EE performance of the proposed joint schemes for multiuser UAV-mmWave systems through simulation. Unless otherwise specified, the main parameters in simulations are listed in Table I. The ground users are uniformly and randomly distributed in a square geographical area of $[0, 200m] \times [0, 200m]$, the carrier frequency is 28 GHz, L_k=3 (k=1,...,K), and σ^2=-104dBm. The simulation results are obtained by 10^4 channel realizations, and are shown in Figs.2-11. In simulation, the computer we used is an Intel Xeon E5-4610 v4 1.80GHz and 32G RAM.

TABLE I
THE SIMULATION PARAMETERS

Parameters	Values
UAV height	$H_u = 200$m
Number of antennas	$M = 32$
Number of users	$K = 3$
minimum rate constraint	$r_0 = 1bps/Hz$
Path-loss exponent	$\alpha_{LoS} = 2$, $\alpha_{NLoS} = 2.9$
Power amplifier efficiency	$\kappa = 0.38$
Power consumption of the baseband	$P_{BB} = 200mW$
Power consumption of the RF chain	$P_{RF} = 300mW$
Power consumption of the phase shifter	$P_{PS} = 40mW$

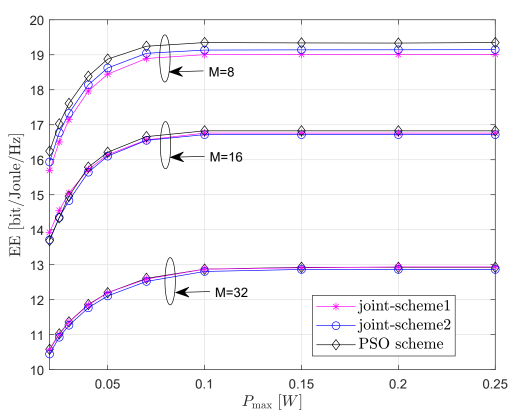

Fig. 2. EE of the system with different antenna numbers

In Fig. 2, we plot the EE of the system with different joint schemes, where the proposed joint-scheme1 and joint-scheme2, the particle swarm optimization (PSO) scheme [41] with 2D search of position as a benchmark are compared, and M=8, 16, 32. From Fig. 2, it is found that the proposed joint-scheme2 can achieve almost the same EE performance as joint-scheme1 for different M. Moreover, these two scheme have the EE very close to the benchmark provided by the PSO scheme, but the formers have lower complexity than the PSO scheme due to the poor computational efficiency of the latter. Besides, with the increase of M, the EE becomes smaller. The reason is that the effect of total power consumption on the EE performance becomes more obvious than the achievable sum rate when M is larger (under this case, total power consumption becomes larger as well since the power consumption of M phase shifter is included, which results in larger power consumption). The results above verifies the effectiveness of the proposed schemes.

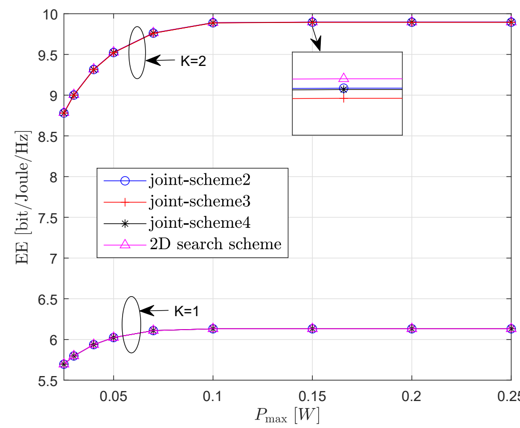

Fig. 3. EE of the system with different user numbers

Fig. 3 illustrates the EE of the system with different numbers of users, where K=1, 2, and three joint design schemes (i.e., joint-scheme2, joint-scheme3 and joint-scheme4) are compared. To assess the validity of the proposed position optimization scheme, the 2D search scheme based on Algorithm 3 is also compared (where the optimal position is attained by the 2D search method). As shown in Fig. 3, the joint-scheme2 achieves higher EE than the joint-scheme3 and joint-scheme4 because near-optimal BF and optimal PA are used. However, the latter two has lower complexity than the former. Besides, the joint-scheme4 has slightly higher EE than the joint-scheme3. This is because the former is more useful for a few number of users, and can obtain near-optimal BF for single user. It is found that joint-scheme2 with our suboptimal position can obtain the EE very close to that with 2D search method, but the complexity is much lower than the latter since the latter uses exhaustive search. Moreover, the same EE is attained for K=1 because the obtained position is also optimal under this case. Furthermore, the EE increases with the increase of K, i.e., the EE with K=2 is higher than that with K=1 due to more users supported. The above results show that the proposed schemes are valid for different numbers of users.

Fig. 4 gives the EE of the system with different BF schemes for different antenna numbers, where M=32, 64, and the joint-scheme2 with sub-BF1, joint-scheme3 with sub-BF2 and joint-scheme4 with sub-BF3 are compared. Also, the joint scheme2 with the BF generated by ABC algorithm (BF-ABC) in [16] is used for comparison. It is observed that the proposed joint-scheme2 with sub-BF1 can obtain almost the same EE as that with BF-ABC, but the complexity is lower than the latter due to higher complexity of this smart algorithm, which can also be seen from the run time in Table II. Moreover,

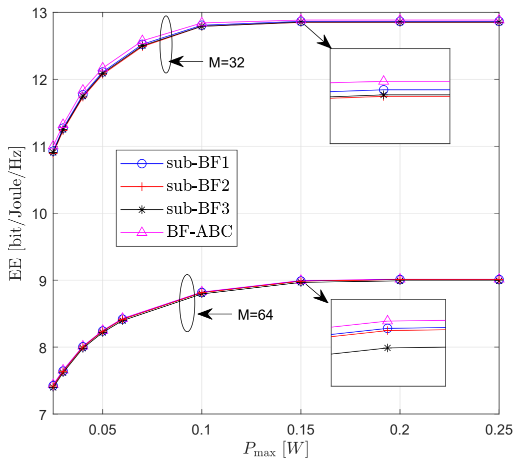

Fig. 4. EE of the system with different BF schemes

TABLE II
COMPARISON OF AVERAGE RUN TIME FOR DIFFERENT SCHEMES

	average run time		average run time
sub-BF1	0.56s	sub-BF2	0.041s
sub-BF3	0.017s	BF-ABC	10.61s

the joint-scheme2 slightly outperforms the joint-scheme3 and joint-scheme4 since near-optimal BF is employed, but its complexity is higher than the latter two because three-loop iterations are needed. Besides, for $M = 64$, joint-scheme3 has slightly higher EE than joint-scheme4, but for $M = 32$, the latter has slightly higher EE than the former.

In Table II, we give the comparison of average run time of four schemes in Fig. 4. From Table II, it is found that the BF-ABC scheme needs longer run time because of much higher complexity. Moreover, the sub-BF1 also has longer run time than the sub-BF2 and sub-BF3 due to the three-loop iterations. Besides, the sub-BF3 has less run time than the sub-BF2 since closed-form BF can be provided. The above results is in accordance with the complexity analysis in Section VI.

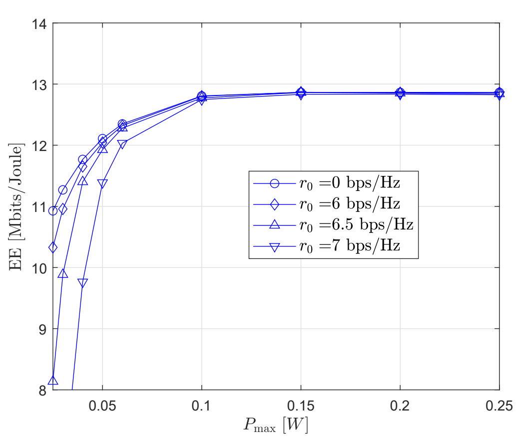

Fig. 5. EE of the system with different rate constraints

Fig. 5 depicts the EE of the system with joint-scheme2 for different minimum rate requirements, where r_0=0, 6, 6.5, 7bps/Hz. As shown in Fig. 5, the EE decreases as the minimum rate constraint r_0 increases. This is because more power will be required to maintain higher rate constraint with the increase of r_0, which may lead to exceed the maximum power constraint resulting in no feasible solution and reduction in average EE. Besides, the system without rate constraint has higher EE than that with rate constraint at low P_{max} since the latter has the limitation of minimum rate. Especially when r_0 is larger, the superiority will become more obvious. However, with the P_{max} increasing, the latter has almost the same EE as the former. The reason is that latter can obtain higher data rate at large P_{max}, and satisfy the r_0 requirement automatically. As a result, almost the same EE can be attained.

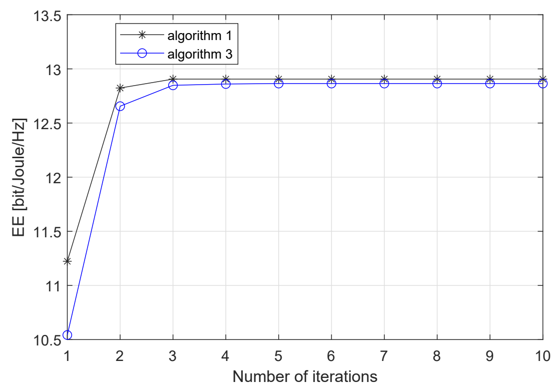

Fig. 6. EE versus number of iterations

Fig. 6 illustrates the convergence behavior of the outer iterations in Algorithm 1 and Algorithm 3, where the EE versus the number of iterations is provided, and we set P_{max}=0.1W. As shown in Fig. 6, the EE is gradually increasing and finally saturated as the number of iteration increases. Thus, the BCD convergence of Algorithm 1 and Algorithm 3 are guaranteed. Moreover, after some iterations, these two algorithms can converge to their respective optimal values, which are almost the same, but the required iterations are different. The Algorithm 1 needs about 3 iterations to converge, and the Algorithm 3 needs about 4 iterations to converge. Because the inner-layer iteration of Algorithm 3 is not considered, the difference of the iterative numbers of these two algorithms is not large. The results further indicate that these two algorithms are valid.

Fig. 7 shows the EE of the system with joint-scheme4 under no rate constraint, where conventional equal power scheme ($i.e., p_1 = ... = p_K = P_{max}/K$) and random position scheme (i.e., the UAV position is randomly generated) are compared. For equal power scheme, the position is obtained by Algorithm 1 and BF scheme is from sub-BF3. While for random position scheme, the power is generated by Algorithm 1 and and BF scheme is from sub-BF3. Form Fig. 7, it is found that the proposed scheme can obtain higher EE than the equal power scheme and random position scheme because the optimized power and position are applied. Moreover, the equal power scheme has the EE performance close to that of the proposed scheme at small P_{max}, but it has obvious performance degradation at large P_{max} since more power is consumed with the increase of P_{max}. Besides, due to

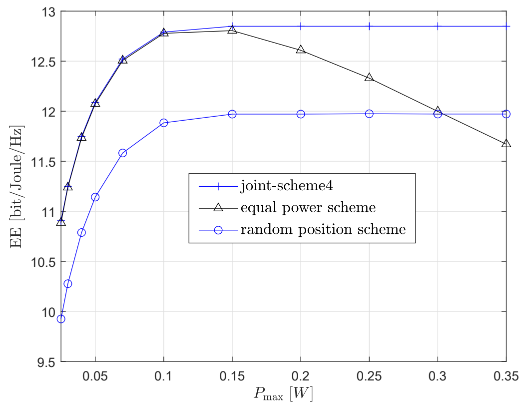

Fig. 7. EE of the system with different schemes

the randomness of UAV position, the EE performance of random position scheme is obviously worse than that of the proposed scheme and equal power scheme. When P_{max} is large, however, it performs better than the equal power scheme.

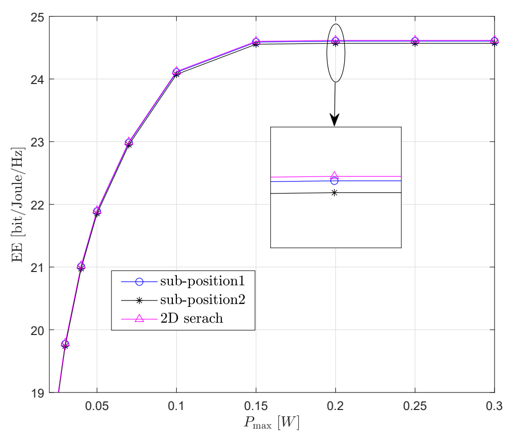

Fig. 8. EE of the system with different position schemes

Fig. 8 provides the EE performance of the system with Algorithm 3 under no rate constraint, where different position optimization schemes, that is, the 2D search based optimal position and the proposed two suboptimal positions (i.e.,(24) and (27), which are referred as 'sub-position1' and 'sub-position2', respectively) are compared, and they are used for the position optimization in Algorithm 3, K=7. As shown in Fig. 8, the proposed 'sub-position1' can obtain almost the same EE performance as the optimal position scheme due to better approximation, the 'sub-position2' also has the performance close to that of the optimal position scheme and 'sub-position2', and small performance loss is found because of inaccurate approximation. However, the proposed two suboptimal positions have lower complexity than the optimal position since 2D exhaustive search is not needed.

In Fig. 9 and Fig. 10, we give the EE performance of the system with joint-scheme5 for only LoS and NLoS components, respectively, where two BF schemes, i.e., sub-BF1 and sub-BF3 are used for BF design in joint-scheme5, K=7, and equal

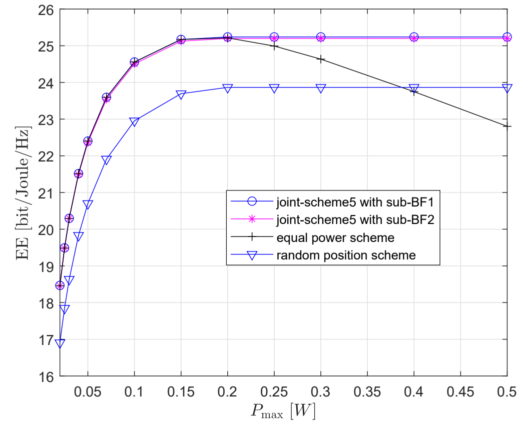

Fig. 9. EE of the system with LoS component only

power scheme and random position scheme are compared. From Fig. 9 and Fig. 10, it is found that the proposed joint-scheme5 is effective, which has higher EE than the equal power and random position schemes due to its optimized resource allocation. Moreover, the joint-scheme5 with sub-BF3 also obtains the EE performance close to that with sub-BF1 but with lower complexity. The results above show that the proposed joint-scheme5 for the system with only LoS or NLoS components is also valid in EE improvement.

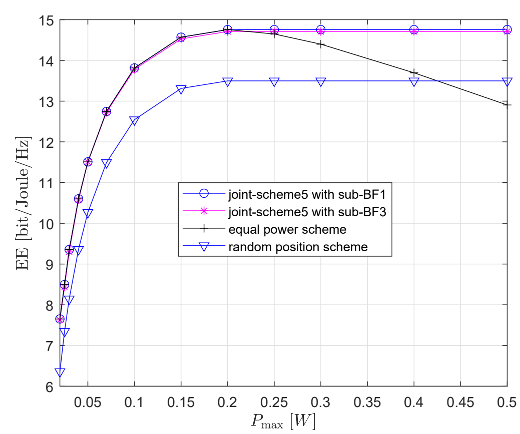

Fig. 10. EE of the system with NLoS component only

In Fig. 11, we plot the EE performance of the system with the proposed schemes for different user numbers, where the joint-scheme1 and joint-scheme2 are compared, and the user' number is set as K=6, 7, 8. As illustrated in Fig. 11, the proposed joint-scheme1 and joint-scheme2 can achieve almost the same performance for more user numbers. Moreover, with the number of user increasing, the EE performance is effectively increased because more users can be supported. Namely, the system with K=8 has higher EE than that with K=7, and the system with K=7 has higher EE than that with K=6. These results indicate that the proposed schemes are also valid for large user number.

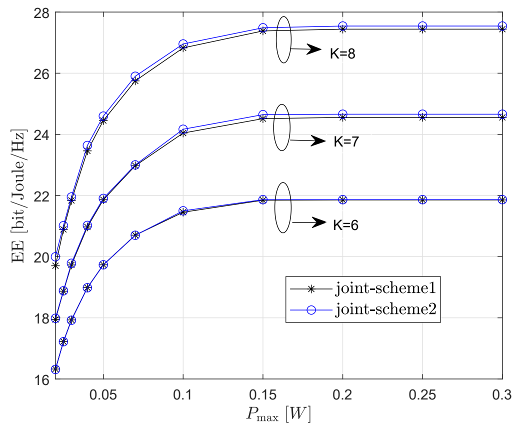

Fig. 11. EE of the system with different user numbers

VIII. Conclusion

The joint design of BF, positioning and PA is studied for maximizing the EE of UAV-mmWave system under the constraints of maximum power, minimal rate, CM and position range. The joint design scheme with two-step optimization is developed to obtain the optimized BF, position and PA in maximizing the EE. In this scheme, suboptimal position is firstly attained by using the first-step optimization. With the obtained position, near-optimal BF is designed given the PA. Then, optimal PA with closed-form expression is derived based on the obtained position and BF. Finally, the near-optimal joint scheme is presented by using the BCD method. To reduce the complexity, two suboptimal BF schemes with single-loop iteration and closed-form solution are also respectively derived. With these two BFs, two suboptimal joint schemes are proposed. To simplify two-step optimization, the joint BF, position and PA with one-step optimization is also designed for two special cases, i.e., only LoS path or NLoS path exists. Simulation results show that the proposed joint schemes are effective, and they can obtain superior EE performance over conventional equal power scheme and random position scheme.

Appendix A
Feasibility analysis

In this appendix, we give the feasibility analysis of problem (10). When the maximum power P_{max} is small or channel condition is poor, the obtained rate may be lower than the minimal rate r_0, and can not satisfy the requirement of r_0. For this reason, we need to check the feasibility of (10). Specifically, with the constraint $\tilde{C}_2$, we set the user's rate equal to r_0 so that the minimal rate requirement is satisfied. Correspondingly, the required power P_t can be attained as

$$P_t = \sum\nolimits_{k=1}^{K} p_k = \sum\nolimits_{k=1}^{K} \frac{\sigma^2 \rho_0}{b_k |\beta_k|^2}, \tag{75}$$

where $p_k = \sigma^2 \rho_0 / (|\beta_k|^2 b_k)$ is from $\tilde{C}_2$ in (10), and $|\beta_k|^2 = \phi_k d_k^{-\alpha}$. By minimizing the P_t, we can check whether (10) is feasible. Correspondingly, the optimization problem is formulated as

$$\min_{\{b_k\}, x_0, y_0} J_{21} = P_t = \sum\nolimits_{k=1}^{K} \frac{\sigma^2 \rho_0}{b_k |\beta_k|^2} \quad \text{s.t. } C_4, C_5. \tag{76}$$

It is observed that the optimized variables $\{b_k\}, (x_0, y_0)$ in (76) has block structure, so we can use the BCD method to tackle this problem. Firstly, given the position (x_0, y_0), we optimize the beam gain $\{b_k\}$, and corresponding problem (76) is reduced to

$$\begin{aligned} &\min_{\{b_k\}} J_{22} = \sum\nolimits_{k=1}^{K} \frac{\sigma^2 \rho_0}{b_k |\beta_k|^2} \\ &\text{s.t. } C_5 : \sum\nolimits_{k=1}^{K} b_k = M. \end{aligned} \tag{77}$$

Considering that the above problem is convex, we can utilize the Lagrange multiplier method to obtain the optimal solution of $\{b_k\}$. Correspondingly, the Lagrange function is given by

$$\mathcal{L}_2 = \sum\nolimits_{k=1}^{K} \frac{\sigma^2 \rho_0}{b_k |\beta_k|^2} + \omega\left(\sum\nolimits_{k=1}^{K} b_k - M\right). \tag{78}$$

By setting $\partial \mathcal{L}_2 / \partial b_k = 0$, we can obtain the closed-form solution of b_k, i.e.,

$$b_k = \frac{M |\beta_k|^{-1}}{\sum_{k=1}^{K} |\beta_k|^{-1}}. \tag{79}$$

Secondly, based on the obtained $\{b_k\}$, we can optimize the position (x_0, y_0), and corresponding problem (76) is reduced to

$$\begin{aligned} &\min_{x_0, y_0} J_{23} = \sum\nolimits_{k=1}^{K} \frac{\sigma^2 \rho_0}{b_k |\beta_k|^2} \\ &\text{s.t. } C_4. \end{aligned} \tag{80}$$

The above problem is equivalent to problem (26), then we can use (27) and (28) to obtain the solution of (x_0, y_0). With the obtained $\{b_k\}$ and (x_0, y_0), we employ the BCD method to update their value iteratively until they converge. As a result, the optimized $\{b_k^*\}$ and (x_0^*, y_0^*) are attained. Based on this, the optimized PA $p_k^* = \sigma^2 \rho_0 / (|\beta_k^*|^2 b_k^*)$. Hence, when the obtained power sum $\sum_{k=1}^{K} p_k^*$ satisfies P_{max} constraint, the (10) can have feasible solution.

Appendix B
Proof of Lemma 1

Proof: Reformulate (48) as

$$(t - t_1)(t - x_2)(t - t_3) = 0. \tag{81}$$

Then we have:

$$t_1 t_2 t_3 = -D/A \tag{82}$$

Since $\frac{D}{A} < 0$, then $t_1 t_2 t_3 > 0$. Let $\triangle = (\frac{\mu}{2})^2 + (\frac{\tau}{3})^3$ be the discriminant of (48), then the three solutions can be divided into two different cases as follows:

(1) If $\triangle > 0$, then (48) has a real-valued solution and a pair of conjugate complex solutions. Since $t_1 t_2 t_3 > 0$, the real-valued solution must be positive.

(2) If $\triangle \leq 0$, then (48) has three real-valued solutions. Since $t_1 t_2 t_3 \geq 0$, there are two cases of solution, i.e., 1)

one positive solution and two negative solutions, and 2) three positive solutions.

Therefore, if $A > 0, D < 0$, then Eq.(48) has one positive real-valued solution or three positive real-valued solutions. ■

ACKNOWLEDGMENTS

The authors would like to thank the anonymous reviewers for their valuable comments which improve the quality of this paper.

REFERENCES

[1] X. Wang, L. kong, F. Kong, F. Qiu, M. Xia, S. Arnon, G. Chen, "Millimeter wave communication: a comprehensive survey," *IEEE Communications Surveys & Tutorials*, vol. 20, no. 3, pp. 1616-1653, 2018.

[2] Z. Xiao, L. Zhu, Y. Liu, P. Yi, R. Zhang, X.-G. Xia, and R. Schober, "A Survey on millimeter-wave beamforming enabled UAV communications and networking," *IEEE Commun. Surveys Tuts.*, Early access, 2021.

[3] C. G. Ruiz, A. Pascual-Iserte and O. Muioz, "Analysis of blocking in mmWave cellular systems: application to relay positioning," *IEEE Trans. Commun.*, vol. 69, no. 2, pp. 1329-1342, Feb. 2021.

[4] L. Zhu, J. Zhang, Z. Xiao, X.-G. Xia, R. Zhang, "Multi-UAV aided millimeter-wave networks: positioning, clustering, and beamforming," *IEEE Trans. Wireless Commun.*, Early access, 2021.

[5] Y. Ji, Z. Yang, H. Shen, W. Xu, K. Wang and X. Dong, "Multicell edge coverage enhancement using mobile UAV-relay," *IEEE Internet Things J.*, vol. 7, no. 8, pp. 7482-7494, Aug. 2020.

[6] A. Ranjha and G. Kaddoum, "URLLC-enabled by laser powered UAV relay: A quasi-optimal design of resource allocation, trajectory planning and energy harvesting,"*IEEE Trans. Veh. Technol.*, Early access, 2021.

[7] C. Zhang, L. Zhang, L. Zhu, T. Zhang, Z. Xiao and X. -G. Xia,"3D deployment of multiple UAV-mounted base stations for UAV communications," *IEEE Trans. Commun.*, vol. 69, no. 4, pp. 2473-2488, Apr. 2021.

[8] K. Chen, Y. Wang, J. Zhao, X. Wang and Z. Fei, "URLLC-oriented joint power control and resource allocation in UAV-assisted networks," *IEEE Internet Things J.*,, vol. 8, no. 12, pp. 10103-10116, June 2021.

[9] J. Zhao, J. Liu, J. Jiang and F. Gao,"Efficient deployment with geometric analysis for mmWave UAV communications," *IEEE Wireless Commun. Lett.*, vol. 9, no. 7, pp. 1115-1119, Jul. 2020.

[10] S. Kumar, S. Suman and S. De, "Dynamic resource allocation in UAV-enabled mmWave communication networks," *IEEE Internet Things J.*, vol. 8, no. 12, pp. 9920-9933, Jun. 2021.

[11] J. Du, W. Xu, Y. Deng, A. Nallanathan, and L. Vandendorpe, "Energy-saving UAV-assisted multiuser communications with massive MIMO hybrid beamforming," *IEEE Commun. Lett.*, vol. 24, no.5, pp.1100-1104, May 2020.

[12] A. Ranjha and G. Kaddoum, "Quasi-optimization of distance and blocklength in URLLC aided multi-hop UAV relay links," *IEEE Wireless Commun. Lett.*, vol. 9, no. 3, pp. 306-310, March 2020.

[13] A. Ranjha and G. Kaddoum, "URLLC facilitated by mobile UAV relay and RIS: a joint design of passive beamforming, blocklength, and UAV positioning," *IEEE Internet Things J.*, vol. 8, no. 6, pp. 4618-4627, March 2021

[14] H. Ren, Q. Cheng, K. Xue, W. Chen, M. Debbah, and Z. Han, "Millimeter-wave networking in the sky: A machine learning and mean field game approach for joint beamforming and beam-steering," *IEEE Trans. Wireless Commun.*, vol. 19, no. 10, pp. 6393-6408, Oct. 2020.

[15] J. Wang, R. Han, L. Bai, T. Zhang, J. Liu and J. Choi, "Coordinated beamforming for UAV-aided millimeter-wave Communications using GPML-based channel estimation," *IEEE Trans. Cognit. Commun. Netw.*, vol. 7, no. 1, pp. 100-109, Mar. 2021.

[16] Z.Xiao, H. Dong, L. Bai, et al., "Unmanned aerial vehicle base station (UAV-BS) eeployment with millimeter-wave beamforming," *IEEE Internet Things J.*, vol.7, no.2, pp.1336-1349, Feb. 2020.

[17] L. Zhu, J. Zhang, Z. Xiao, X. Cao, X. -G. Xia and R. Schober, "Millimeter-wave full-duplex UAV relay: joint positioning, beamforming, and power control," *IEEE J. Sel. Areas Commun.*, vol. 38, no. 9, pp. 2057-2073, Sept. 2020.

[18] S. Zhang, X. Cai, W. Zhou, Y. Wang, "Green 5G enabling technologies: an overview," *IET Commun.*, vol.13, no.2, pp.135-143, 2019.

[19] J. Chakareski, S. Naqvi, N. Mastronarde, J. Xu, F. Afghah and A. Razi, "An energy efficient framework for UAV-assisted millimeter Wave 5G heterogeneous cellular networks," *IEEE Trans. Green Commun. Netw.*, vol. 3, no. 1, pp. 37-44, Mar. 2019.

[20] A. Ranjha and G. Kaddoum, "Quasi-optimization of uplink power for enabling green URLLC in mobile UAV-assisted IoT networks: A perturbation-based approach," *IEEE Internet Things J.*, vol. 8, no. 3, pp. 1674-1686, Feb. 2021.

[21] Y. Shi, M. Q. Hamdan, E. Alsusa, K. A. Hamdi and M. W. Baidas, "A decoupled access scheme with reinforcement learning power control for cellular-enabled UAVs," *IEEE Internet Things J.*, Early access, 2021.

[22] Z. Xiao, L. Zhu, J. Choi, P. Xia, and X. G. Xia., "Joint power allocation and beamforming for non-orthogonal multiple access (NOMA) in 5G millimeter wave communications," *IEEE Trans. Wireless Commun.*, vol. 17, no. 5, pp. 2961-2974, May 2018.

[23] X. Yu, X. Dang, B. Wen, S. Leung and F. Xu, "Energy-efficient power allocation for millimeter-wave system with non-orthogonal multiple access and beamforming," *IEEE Trans. Veh. Technol.*, vol. 68, no. 8, pp. 7877–7889, Aug. 2019.

[24] C.-L. He, B. Sheng, P.-C. Zhu, X.-H. You, and G. Y. Li, "Energy and spectral efficiency tradeoff for distributed antenna systems with proportional fairness," *IEEE J. Sel. Areas Commun.*, vol. 31, no. 5, pp. 894-902, May. 2013.

[25] X.Yu, T.Teng, X.Dang, S.-H. Leung, and F.Xu, "Joint power allocation and beamforming for energy-efficient design in multiuser distributed MIMO systems," *IEEE Trans. Commun.*, vol.69, no.6, pp.4128-4143, June 2021.

[26] J.Lee, G.T.Gil, and Y.H.Lee, "Exploiting spatial sparsity for estimating channels of hybrid MIMO systems in millimeter wave communications," in *Global Communications Conference*, 2014, pp. 3326-3331.

[27] L. Zhu, J. Zhang, Z. Xiao, X. Cao, D. Wu, X.-G. Xia, "Millimeter-wave NOMA with user grouping, power allocation and hybrid beamforming,"*IEEE Trans. Wireless Commun.*, vol.18, no.11, 5065-5079, 2019.

[28] J.Guo, Q.Yu, W.Meng, and W.Xiang,"Energy-efficient hybrid precoder with adaptive overlapped subarrays for large-array mmWave systems,"*IEEE Trans. Wireless Commun.*, vol.19, no.3, pp. 1484-1502, 2020.

[29] S. Buzzi and C. DAndrea, "Energy efficiency and asymptotic performance evaluation of beamforming structures in doubly massive MIMO mmWave systems,"*IEEE Trans. Green Commun. Netw.*, vol. 2, no. 2, pp.385-396, Jun. 2018.

[30] P. Wang, J. Fang, X.Yuan, Z. Chen, and H. Li, "Intelligent reflecting surface-assisted millimeter wave communications: joint active and passive precoding design," *IEEE Trans. Veh. Technol.*, vol. 66, no. 12, pp. 14960–14973, Dec. 2020.

[31] N. Tafintsev, M. Gerasimenko, D. Moltchanov, et al., "Improved network coverage with adaptive navigation of mmWave-based drone-cells," in *Proc. IEEE Globecom Workshops (GC Wkshps)*, Dec. 2018, pp. 1-7.

[32] L. Dai, B. Wang, M. Peng, and S. Chen, "Hybrid precoding-based millimeter-wave massive MIMO-NOMA with simultaneous wireless information and power transfer," *IEEE J. Sel. Areas Commun.*, vol. 37, no. 1, pp. 131-141, Jan. 2019.

[33] A. Beck and L. Tetruashvili, "On the convergence of block coordinate descent type methods," *SIAM J. Optim.*, vol. 23, no. 4, pp. 2037-2060, 2013.

[34] S. J. Wright, "Coordinate descent algorithms," *Mathematical Programming*. vol.151, no.1, pp. 3-34. June 2015.

[35] A. Jeffrey and D. Zwillinger, Table of Integrals, Series, and Products, 7th ed., New York, NY, USA: Academic, 2007.

[36] M. R. Akdeniz, Y. Liu, M. K. Samimi, et al., "Millimeter wave channel modeling and cellular capacity evaluation," *IEEE J. Sel. Areas Commun.*, vol. 32, no. 6, pp. 1164-1179, Jun. 2014.

[37] W. Dinkelbach, "On nonlinear fraction programming," *Management Science*, vol 13, no. 7, pp. 492-298, 1967.

[38] R. M. Corless, G. H. Gonnet, D. E. G.Hare, et al., "On the lambert w function," *Adv. Comput. Math.*, vol.5, no.1, pp. 329-359, 1996.

[39] M. S. Bazaraa, H. D. Sherali, and C. M. Shetty, *Nonlinear programming: theory and algorithms*. John Wiley & Sons, 2013.

[40] Y. Sun, P. Babu, and D. P. Palomar, "Majorization-minimization algorithms in signal processing, communications, and machine learning," *IEEE Trans. Signal Process.*, vol. 65, no. 3, pp. 794-816, 2017.

[41] R. Poli, J. Kennedy, and T. Blackwell, "Particle swarm optimization," *Swarm Intell.*, vol. 1, no. 1, pp. 33–57, 2007.